Geochimica et Cosmochimica Acta 354 (2023) 197–210

Contents lists available at ScienceDirect

Geochimica et Cosmochimica Acta

journal homepage: www.elsevier.com/locate/gca

Marine nitrogen cycling dynamics under altering redox conditions: Insights from deposition of sapropels S1 and the ambiguous S2 in the Eastern Mediterranean Sea

Zoë R. van Kemenade [a,*], Anna Cutmore [a], Rick Hennekam [a], Ellen C. Hopmans [a], Marcel T.J. van der Meer [a], Meryem Mojtahid [b], Frans J. Jorissen [b], Nicole J. Bale [a], Gert-Jan Reichart [a,c], Jaap S. Sinninghe Damsté [a,c], Darci Rush [a]

[a] NIOZ Royal Netherlands Institute for Sea Research, Landsdiep 4, 1797 SZ 't Horntje, the Netherlands
[b] Université d'Angers, Nantes Université, Le Mans Université, CNRS, Laboratoire de Planétologie et Géosciences, LPG UMR 6112, 49000 Angers, France
[c] Department of Earth Sciences, Utrecht University, Princetonlaan 8a, 3584 CB Utrecht, the Netherlands

ARTICLE INFO

Associate editor: Haojia Ren

Original content: Marine nitrogen cycling dynamics under altering redox conditions: insights from deposition of sapropels S1 and the ambiguous S2 in the Eastern Mediterranean Sea (Original data)
Marine nitrogen cycling dynamics under altering redox conditions: insights from deposition of sapropels S1 and the ambiguous S2 in the Eastern Mediterranean Sea (Original data)

Keywords:
Marine nitrogen cycle
Sapropel
Eastern Mediterranean Sea
Lipid biomarkers
Anoxic events

ABSTRACT

The eastern Mediterranean Sea (EMS) sedimentary record is periodically interspersed with organic-rich 'sapropel' layers. Sapropels are characteristic of basin-wide anoxic events, triggered by precession-forced insolation maxima. Relatively subdued insolation maxima, however, are not always expressed as distinct sapropel events. The EMS sedimentary record is thus useful to investigate feedbacks between marine anoxia and the nitrogen (N) cycle and offers an analogue for modern deoxygenation and past oceanic anoxic events. To this end, we investigated a ~68 kyr sedimentary record from the EMS containing the well-established sapropel S1 (deposited in two phases: S1a [~10.5–8.5 ka BP] and S1b [~7.8–6.1 ka BP]) and sediments timed to the ambiguous S2 sapropel (~53 ka BP). We used lipid biomarkers of microorganisms to reconstruct key N-cycle components: (1) anaerobic ammonium oxidation (anammox) using ladderanes and a stereoisomer of bacteriohopanetetrol (BHT-*x*), (2) dinitrogen gas (N_2) fixation using heterocyte glycolipids, and (3) nitrification by Thaumarchaeota using crenarchaeol. Additionally, benthic foraminifera and trace metals (U, Mo, Mn) were used to reconstruct redox conditions. During S1a, abundances of Thaumarchaeota increased, likely promoted by elevated high-nutrient freshwater discharge. At this time, a combination of phosphorus supply and intensified loss of bioavailable N via water column anammox, may have reinforced anoxia by favoring diatom-diazotroph associations. During S1b, anammox is equally intense. Yet, no positive feedback on N_2-fixation is observed, likely because diazotrophs were phosphorus limited. Instead, anammox may have provided negative feedback on anoxia by quenching primary production. Ladderanes suggest additional episodes of anammox between ~69 to 39 cal ka BP, corresponding to brief periods of water column deoxygenation. Anoxia likely occurred at the sediment–water interface in S2-timed sediments (53–51 cal ka BP). During these episodes, ladderanes co-occur with the later eluting BHT-34*R* stereoisomer. $\delta^{13}C_{BHT\text{-}34R}$ indicate an anammox source, potentially synthesized by marine sedimentary anammox bacteria. No corresponding increase in diatom-diazotroph associations is observed, likely due to the oligotrophic conditions and the limited effect of sedimentary anammox on N-availability in the euphotic zone. Our results highlight various modes of operation of the N-cycle at different degrees of deoxygenation, which depend amongst others on nutrient-availability and the niche-segregation of N-loss and N_2-fixating microorganisms.

1. Introduction

In the Eastern Mediterranean Sea (EMS), the cyclic occurrence of dark, organic-matter rich sediment layers, known as sapropels, are diagnostic of basin-wide anoxic events. Sapropels typically have an elevated total organic carbon (TOC) content of >2% (Kidd et al., 1978), which has been attributed to: (1) enhanced primary productivity in response to increased terrestrial nutrient-runoff (Calvert, 1983), (2)

* Corresponding author.
E-mail address: zoe.van.kemenade@nioz.nl (Z.R. van Kemenade).

https://doi.org/10.1016/j.gca.2023.06.018
Received 28 October 2022; Accepted 16 June 2023
Available online 19 June 2023

better preservation of organic matter (OM) under anoxic conditions (Rossignol-Strick, 1982), or (3) a combination of both (Howell and Thunell, 1992). The timing of sapropel deposition is associated with precession-forced insolation maxima, driving an intensified North-African monsoon (Rossignol-Strick, 1985). The strengthened monsoonal climate fueled increased freshwater discharge into the Mediterranean Sea, causing density stratification and increased input of nutrients. The resulting cessation of the thermohaline deep-water mass circulation ultimately led to the formation of oxygen depleted deep-waters (*e.g.*, Rossignol-Strick, 1982; Rohling et al., 2015). Because of their (quasi-) periodicity and excellent preservation, sapropels are ideally suited to evaluate the marine nitrogen (N) cycle under low oxygen conditions. Furthermore, throughout the late Quaternary, not all precession minima are associated with distinct sapropel deposits. These periods of likely less intense deoxygenation have been poorly studied for N-cycle dynamics, despite potentially providing useful information on feedback mechanisms.

At the time of the most recent precession minimum, during which sapropel S1 was deposited (~10.5–6.1 ka BP; Grant et al., 2016), evidence for bottom water anoxia, based on redox sensitive trace metals (*e.g.*, molybdenum, 'Mo' and uranium, 'U'; *e.g.*, Thomson et al., 1995) and benthic foraminifer assemblages (*e.g.*, Abu-Zied et al., 2008) is clear. In contrast, during the precession minimum at ~60 ka BP (Laskar et al., 2004), the corresponding sapropel unit (S2), has not been distinguished unequivocally based on redox and paleo-productivity proxies (*e.g.,* the barium to aluminum ratio, 'Ba/Al'; van Santvoort et al., 1997). Yet, around ~55–52 cal ka BP, a minimum $\delta^{18}O$ event has been recorded in Soreq cave spaleothems (Bar-Matthews and Ayalon, 2007), and in multiple cores recovered from the Levantine Basin (Vergnaud-Grazzini et al., 1977; Rossignol-Strick, 1982; Cornuault et al., 2016; this study), which have been associated with insolation driven increased rainfall (Rossignol-Strick, 1982). Also, a weakened intermediate thermohaline circulation at ~53–51 ka BP (*i.e.*, the approximate timing of S2; Muerdter et al., 1984), is thought to have resulted in reduced bottom water oxygenation in the EMS at this time (Di Donato et al., 2022). As such, some reduced ventilation may be inferred, but the corresponding levels of deoxygenation and associated N-cycling dynamics are still poorly elucidated. Thus, by reconstructing key processes of the N-cycle and redox conditions during the S1 and S2 intervals (from here on referred to as 'S2' due to its ambiguity), potential feedbacks between the N cycle and anoxia, may be exposed.

The availability of dissolved oxygen has a large impact on how N is cycled in marine systems (Fig. 1a). Lipid biomarkers of organisms involved in the N cycle are useful tools in the reconstruction of the different components of the marine N cycle and associated redox conditions (Fig. 1b). Under anoxic conditions, bioavailable N (*i.e.*, nitrate 'NO_3^-', nitrite 'NO_2^-' and ammonium 'NH_4^+'), is lost through anaerobic ammonium oxidation (anammox; van de Graaf et al., 1997; Kuypers et al., 2003) and denitrification (Kuenen and Robertson, 1988). Ladderane lipids (Sinninghe Damsté et al., 2002c) have been used as biomarker lipids for the past presence of anammox bacteria during sapropel deposition (Rush et al., 2019). In addition, while bacteriohopanetetrol (BHT)-34*S* is ubiquitously synthesized by bacteria, a later eluting stereoisomer (BHT-*x*) has been proposed to be uniquely synthesized by marine anammox bacteria, *i.e.*, *Ca.* Scalindua spp. (Rush et al., 2014; Schwartz-Narbonne et al., 2020). Since then, BHT-*x* has been successfully applied as a biomarker for anammox in a modern marine setting (van Kemenade et al., 2022) and in late Quaternary and Pliocene sapropels (Rush et al., 2019). A third BHT stereoisomer (BHT-34*R*) is known to be synthesized by freshwater anammox bacteria and various aerobic terrestrial microbial species (Peiseler and Rohmer, 1992; Rosa-Putra et al., 2001; Schwartz-Narbonne et al., 2020).

In Plio-Pleistocene sapropels, lipid biomarkers have also been used to detect the oxidation of ammonium (NH_4^+) to nitrite (NO_2^-) by Thaumarchaeota (Menzel et al., 2006; Castañeda et al., 2010; Polik et al., 2018), using crenarchaeol (Sinninghe Damsté et al., 2002b) and N_2-fixation by heterocytous cyanobacteria (Bale et al., 2019; Elling et al., 2021), using heterocyte glycolipids (HGs). Pentose HGs (C_5 HGs) are synthesized by cyanobacteria living in symbiosis with diatoms (diatom-diazotroph associations, 'DDAs'; Schouten et al., 2013; Bale et al., 2015), while hexose HGs (C_6 HGs) are synthesized by freshwater/brackish cyanobacteria of the order Nostocales (Bauersachs et al, 2009; Wörmer et al., 2012). The occurrence of DDAs during sapropel events has been proposed to sustain high mineralization rates, hereby providing a positive feedback on anoxia (Kemp et al., 1999; Sachs and Repeta, 1999). Unsaturated BHT-cyclitol ether (BHT-CE), amongst others synthesized by the filamentous N_2-fixating non-heterocytous cyanobacterium *Trichodesmium* sp. (Talbot et al., 2008), has also been used to infer past N_2-fixation (Handley et al., 2010). Applying lipid biomarkers may thus provide us with detailed information on the evolution of the various components of the marine N cycle during sapropel formation.

Here, we explore a ~68 kyr sedimentary record from the EMS

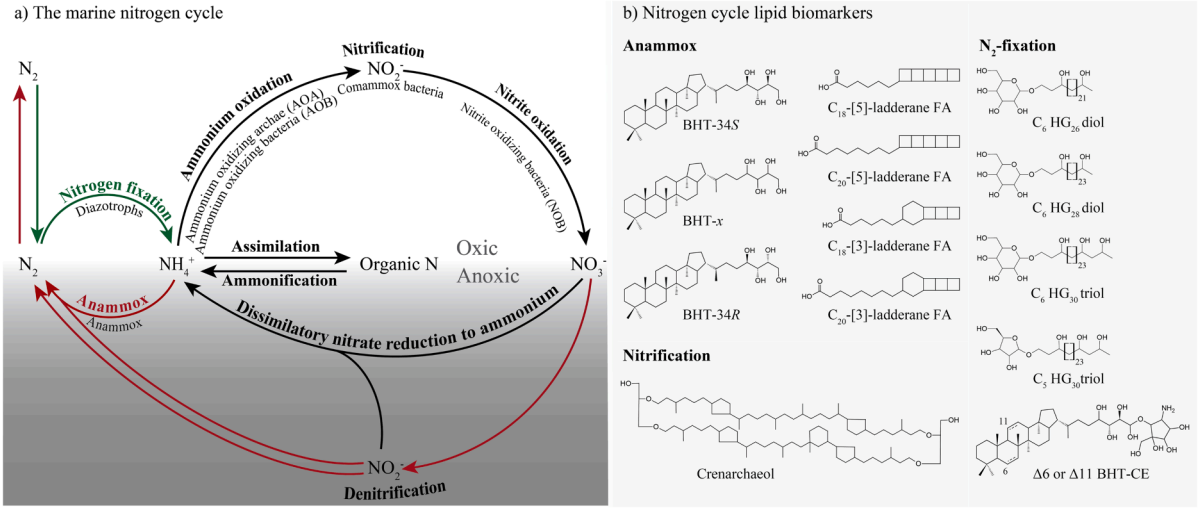

Fig. 1. a) The marine nitrogen (N) cycle. Red arrows indicate the N-loss processes anammox and denitrification. Green arrows indicate N_2-fixation. Key microorganisms associated with a specific pathway are indicated. b) Lipid biomarkers of N-cycling microorganisms applied in this study. Anammox biomarkers: stereoisomers of bacteriohopanetetrol (BHT-34*S*, BHT-*x* and BHT-34*R*), and ladderane fatty acids (FAs) with 5 or 3 cyclobutane moieties and 18 or 20 carbon atoms. Nitrification biomarker: crenarchaeol. Diazotrophy biomarkers: heterocyte glycolipids (HGs) with C_6 or C_5 sugar head groups and alternating C_{26} to C_{30} alkyl chain-lengths and Δ6 or Δ11 BHT-cyclitol ether (BHT-CE).

(64PE406-E1; Fig. 2), which includes the well-established Holocene sapropel S1 as well as the ambiguous 'S2' event of the late Pleistocene. We provide an overview of the N cycle and associated redox conditions, using a broad scope of lipid biomarkers (Fig. 1b) and compound specific carbon (C) and bulk sediment C and N stable isotopes. Moreover, complementary data in this core obtained from bulk sedimentary redox-sensitive trace metals (Mo, U, and manganese to Al, Mn/Al), Ba/Al ratio (partially published earlier in: Hennekam et al., 2020; Clarkson et al., 2021), and foraminiferal assemblages provide additional insights in the redox conditions and productivity during the studied interval. Comparing the different nitrogen–oxygen feedback modes occurring within and between the more intensely deoxygenated S1 and the ambiguous 'S2' ultimately allows us to constrain the feedback of N cycling processes and redox conditions. This provides further insights on biogeochemical responses to marine deoxygenation.

2. Materials and methods

2.1. Sample collection and chronology

A multicore (containing sapropel S1) and piston core (containing onset S1 and 'S2') were collected during the Netherlands Earth System Science Centre (NESSC) research cruise (64PE406) onboard the *R/V* Pelagia, and are collectively referred to as core 64PE406-E1. The cores were recovered in January 2016 at site 64PE406-E1 (33°18.14898′N, 33°23.71998′E; water depth 1760 m below sea surface 'mbss') in the Levantine basin, located in the EMS (Fig. 2). For biomarker and bulk isotope analysis, a total of 49 samples were collected from core 64PE406-E1, forming a (near-)continuous record of the last ~68 kyr, which includes the two most recent insolation maxima (Fig. 3a). High resolution sampling was conducted between 5–15 cal ka BP (16 samples; covering S1) and between 49–59 cal ka BP (18 samples; covering 'S2'). Sediments were freeze-dried and stored at −40 °C until further analysis.

The age model (see supplementary material S1.1 for details) of multicore 64PE406-E1-MC and piston core 64PE406-E1-PC was obtained by correlating Ba/Al excursions and $\delta^{18}O$ values of *Globigerinoides ruber* to those of other well-dated nearby cores (Grant et al., 2012; Zwiep et al., 2018; Hennekam et al., 2020; Clarkson et al., 2021) and to Soreq speleothem $\delta^{18}O$ (Grant et al., 2012).

2.2. Total organic carbon and total nitrogen

Freeze-dried sediments were analyzed for total organic carbon (TOC), total nitrogen (TN) and their stable isotopic composition, $\delta^{13}C_{TOC}$ and $\delta^{15}N_{TN}$, respectively, using a ThermoScientific Flash EA coupled to a Delta V Plus IRMS. For analysis of TOC and $\delta^{13}C_{TOC}$ (but not TN and $\delta^{15}N_{TN}$), aliquots of freeze-dried sediment were first acidified to remove calcium carbonate ($CaCO_3$), using hydrochloric acid (HCl). Sediment aliquots were weighted into tin capsules before combustion. Isotopic compositions were peak size-corrected and offset-corrected using the following certified standards: benzoic acid ($\delta^{13}C$, −27.4; C%, 68.80), acetanilide ($\delta^{13}C$, −29.53; C%, 71.09; $\delta^{15}N$, 1.18; N%, 10.36%), urea ($\delta^{15}N$, 20.17; N%, 46.65‰) and casein ($\delta^{15}N$, 5.94; N%, 13.32‰). Isotopic ratios are reported in ‰ relative to Vienna Pee Dee Belemnite (VPDB) for C, and relative to air for N.

2.3. Benthic foraminiferal analysis

Samples from the multi- and piston cores were sieved over 63 and 150 μm meshes for foraminiferal-based analysis. The >150 μm fraction of all key intervals was studied continuously with a 1 cm resolution (supplementary material 1 Table S2). All low oxygen indicators (Jorissen, 1999) were determined at the species level (*Globobulimina* spp., *Chilostomella* spp. *Cassidulinoides bradyi*, *Ellipsopolymorphina fragilis*, *Fursenkoina* spp., *Stainforthia* spp., *Bulimina exilis* and *Bulimina costata*). On the basis of the cumulative percentage of these low oxygen indicator species (LOS), a semi-quantitative index to estimate bottom water oxygenation (BWO), ranging from 0.0 (anoxia) to 1.0 (100% oxygen saturation) was applied (based on Jorissen et al., 2007), using:

$$BWO = e^{(-0.0625 \times \%LOS)} \quad (1)$$

Samples with a total number of foraminifera less than were considered sterile due to anoxia, and BWO was set to zero.

2.4. Lipid extraction, derivatization and analysis

2.4.1. Bligh and Dyer extractions

Sediments were extracted using a modified Bligh and Dyer extraction (BDE) method (Bligh and Dyer, 1959; Sturt et al., 2004; Bale et al., 2021). Homogenized sediments (~2–10 g) were dispersed in a solvent solution of 2:1:0.8 (*v:v;* ~4–20 mL) methanol (MeoH), dichloromethane (DCM) and phosphate buffer. The monophasic mixture was then sonicated for 10 min and centrifuged for 2 min at 3000 rpm after which the supernatant was collected in a centrifuge tube. This procedure was repeated three more times. For the last two repeats, the phosphate buffer was replaced with trichloroacetic acid, after which the supernatant was

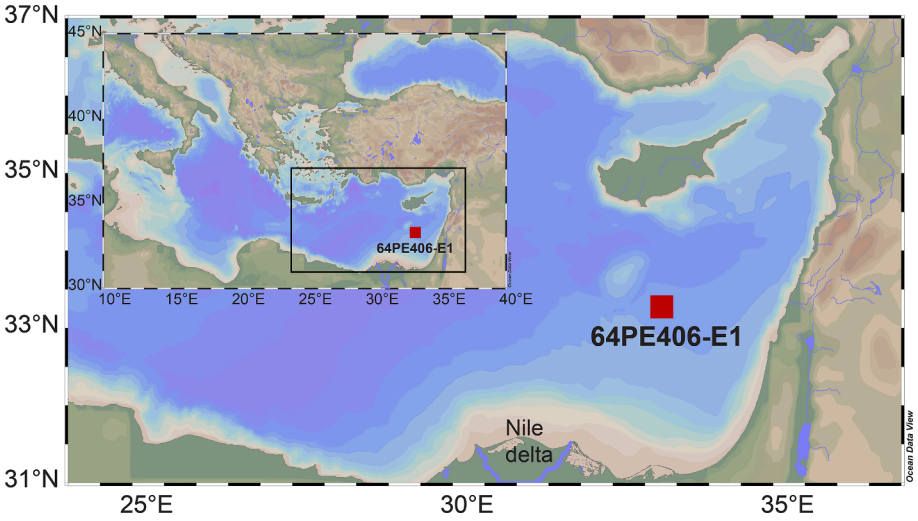

Fig. 2. Location of multi, -and piston core 64PE406-E1 (33°18.14898′N, 33°23.71998′E; indicated with red square) in the Levantine basin, Eastern Mediterranean Sea. Core was recovered from a water depth of 1760 mbss. Rivers are indicated in purple. Map was created using ODV (Schlitzer, R., Ocean Data View, 2021).

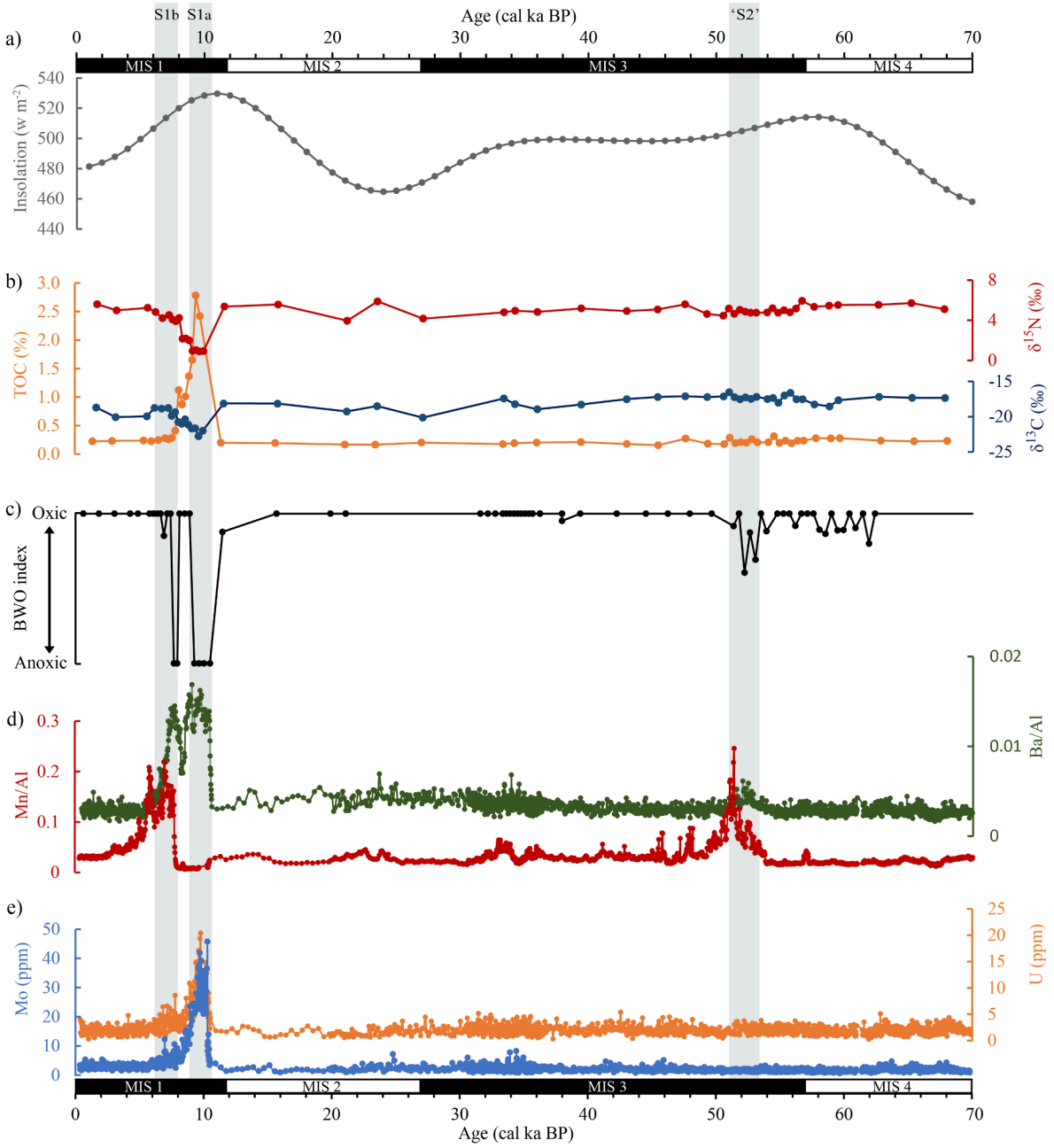

Fig. 3. a) 21st of june 65°n insolation curve (Laskar et al., 2004); data from record 64PE406-E1: b) Total organic carbon (TOC) in orange, sedimentary bulk $\delta^{15}N$ in red and $\delta^{13}C$ in blue; c) Benthic foraminifer derived bottom water oxygen (BWO) estimate; XRF scanning data partially published earlier in Hennekam et al., 2020; Clarkson et al., 2021: d) ratio of Manganese (Mn) to Aluminum (Al) in red and the ratio of Barium (Ba) to Al in green; and e) concentrations of Molybdenum (Mo) in blue and Uranium (U) in orange. Timing of S1a, S1b (Rohling et al., 2015; Grant et al., 2016) and 'S2' (Muerdter et al., 1984), are shown in grey. Glacial and interglacial marine isotope stages are indicated in white and black, respectively.

collected in a separate centrifuge tube. Phase separation was then achieved in the collected supernatant by adding additional DCM and phosphate buffer, to obtain a new ratio of 1:1:0.9 (*v:v*), MeOH, DCM and phosphate buffer, respectively. The biphasic mixture was centrifuged (2 min at 3000 rpm), after which the bottom DCM layer was collected. The remaining solvent phase was washed two more times with DCM, using the same procedure. The combined DCM layers were dried under N_2 gas. Freeze-dried biomass of *Ca.* Scalindua spp. (van de Vossenberg et al., 2008) and *Ca.* Brocadia spp. (Kartal et al., 2007) was extracted similarly, and used as a reference standard for the analysis of C_{18}[3]-, C_{18}[5]-, C_{20}[3]- and C_{20}[5]-ladderanes and BHT stereoisomers.

2.4.2. *Saponification and methylation for ladderane fatty acid analysis*

BDE aliquots were saponified in 2 N potassium hydroxide (in MeOH 96%) by refluxing for 1 h. After, 2 mL of bidistilled water was added to the saponified extracts. The fatty acid (FA) fraction was obtained by acidifying the reaction mixture to a pH of 3 with 2 N hydrochloric acid/MeOH (1:1, *v:v*), and partitioning three times with DCM. The DCM layer was collected each time after centrifuging for 2 min at 3000 rpm. The FA fraction was dried over a sodium sulphate (Na_2SO_4) column, using DCM as an eluant. Following this, the fractions were methylated with diazomethane (CH_2N_2) and air dried overnight. Polyunsaturated fatty acids were removed by eluting the methylated fractions with DCM over a silica impregnated silver nitrate ($AgNO_3$) column. Samples were dissolved in acetone and filtered over 0.45 mm PTFE filters (4 mm; BGB,

USA), before analysis.

2.4.3. Purification and acetylation for $\delta^{13}C_{BHTs}$ compound specific stable isotope analysis

Nine core sediment depths (Table 1) were selected for compound specific $\delta^{13}C$ analysis of BHT-34*S* ($\delta^{13}C_{BHT\text{-}34S}$), BHT-*x* ($\delta^{13}C_{BHT\text{-}x}$) and BHT-34*R* ($\delta^{13}C_{BHT\text{-}34R}$), using the method described in Lengger et al., (2019). BDE aliquots were subjected to column chromatography using Isolute NH_2 500 mg/3mL solid phase extraction (SPE) columns. The columns were preconditioned with 2 × 3 mL hexane. Fraction 1, 2 and 3 were eluted with hexane, DCM, and MeOH, respectively, with the latter containing BHT. All fractions were dried under N_2. Fractions were acetylated using a 1 mL mixture of acetic acid anhydride and pyridine (1:1, *v:v*) at 50 °C for 1 h, and left overnight at room temperature. Acetylated fractions 3 (MeOH) were dried under N_2 and dissolved in ethyl acetate before analysis on the GC-IRMS.

2.4.4. Analysis of intact polar lipids

Deuterated diacylglyceryltrimethylhomoserine (DGTS D-9; Avanti® Polar Lipids, USA) was added as an internal standard to BDE aliquots. Aliquots were dissolved in a MeOH: DCM 9:1 (*v:v*) and filtered over 4 mm True generated cellulose syringe filters (0.45 μm, BGB, USA). Filtered aliquots were analysed on an Agilent 1290 Infinity I ultra-high performance liquid chromatographer (UHPLC) with a thermostatted auto-injector, coupled to a Q Exactive Orbitrap MS with an Ion Max source and heated electrospray ionisation probe (HESI; ThermoFisher Scientific, Waltham, MA), according to Hopmans et al. (2021; modified from Wörmer et al., 2013). Briefly, chromatographic separation was achieved with an Acquity BEH C18 column (2.1 × 150 mm, 1.7 μm, Waters), with A) MeOH / H_2O / formic acid / 14.8 M NH_3aq (85:15: 0.12:0.04 [*v:v*]) and B) IPA / MeOH / formic acid / 14.8 M NH_3aq (50:50:0.12:0.04 [*v:v*]) at a flow rate of 0.2 mL min^{-1}. Compounds were eluted with 5% B for 3 min, followed by a linear gradient to 40% B at 12 min ending at 100% B at 50 min. Lipids were detected using positive ion monitoring of *m/z* 350–2000 (resolution 70,000 ppm at *m/z* 200), followed by data dependent MS^2 (isolation window 1 *m/z*; resolution 17,500 ppm at *m/z* 200) of the 10 most abundant ions.

For the analysis of BHT and unsaturated BHT-CE, optimal fragmentation was achieved with a stepped normalized collision energy of 22.5 and 40 (isolation window 1.0 *m/z*). Identification and integration was based on their exact masses (within 3 ppm) and diagnostic fragmentation spectra (Hopmans et al., 2021). The protonated ($[M+H]^+$ adduct (*m/z* 706.525) was used for integration of unsaturated BHT-CE. The combined mass chromatogram of the ammoniated ($[M+NH_4]^+$) and sodiated ($[M+Na]^+$) adducts (*m/z* 564.499 and *m/z* 569.454, respectively) were used for integration of BHT-34*S*, BHT-*x* and BHT-34*R*. The ratio of BHT-*x* and BHT-34*R* over BHT-34*S* was then calculated as:

$$\text{BHT}-x \text{ ratio} = \frac{\text{BHT}-x}{(\text{BHT}-x + \text{BHT}-34S)} \quad (2)$$

$$\text{BHT}-34R \text{ ratio} = \frac{\text{BHT}-34\text{R}}{(\text{BHT}-34R + \text{BHT}-34S)} \quad (3)$$

For the analysis of HGs and crenarchaeol, optimal fragmentation was achieved with a stepped normalized collision energy of 15, 22.5 and 30 (isolation window 1.0 *m/z*). Identification and integration of analyzed compounds was based on their exact masses (within 3 ppm) and diagnostic fragmentation spectra (Bauersachs et al., 2009; Schouten et al., 2013; Bale et al., 2019). The combined mass chromatograms of the $[M+H]^+$ and $[M+NH_4]^+$ adducts were used to integrate hexose and pentose HGs. Identified and integrated HGs were: C_6 HG_{26} diol (*m/z* 577.467 and *m/z* 594.494), C_6 HG_{28} diol (*m/z* 605.499 and *m/z* 621.517), C_6 HG_{30} triol (*m/z* 649.525 and *m/z* 666.552) and C_5 HG_{30} triol (*m/z* 619.514 and *m/z* 636.541). Mass chromatograms of the $[M+H]^+$, $[M+NH_4]^+$ and $[M+Na]^+$ adducts and their first isotopologue were used to integrate crenarchaeol (*m/z* 1292.244, 1293.252, *m/z* 1309.271, 1310.279, *m/z* 1314.226, 1315.234).

The integrated peaks were corrected for matrix effects and variations in MS performance using the internal DGTS-D9 standard. Due to a lack of authentic standards for absolute quantifications, concentrations are reported as their relative integrated peak area response unit (ru), and normalized against their accumulation rate (ru g^{-1} cm^{-2} kyr^{-2}). Normalized concentrations per gram TOC (ru $gTOC^{-1}$) are also reported (supplementary material 1 Fig. S2). Although this does not allow for quantification of absolute concentrations, it does allow for relative quantification, as the response factor should be identical across the sample set.

2.4.5. Analysis of ladderane fatty acids

Filtered FAME fractions were analyzed on an Agilent 1290 Infinity I UHPLC equipped with a thermostatted auto-injector and column oven, coupled to a Q Exactive Plus Orbitrap MS, with a positive ion

Table 1
$\delta^{13}C$ values [‰ V-PDB] and standard deviations (s.d.; 1-sigma) of (from left to right) BHT-34*S*, BHT-*x*, BHT-34*R* and TOC in nine samples from core 64PE406-E1, with corresponding age (in cal ka BP). Additionally, $\delta^{13}C$ values for BHT-*x* and BHT-34*R* were determined for *Ca.* Scalindua spp. and *Ca.* Brocadia spp., biomass (above the upper dotted line) recovered from an anoxic sequencing batch reactor at Radboud University, the Netherlands. Samples below the lower dotted line reflect median values of entire datasets, with datasets from a: this study, recovered from core PE406-E1 in the Levantine basin; b: Lengger et al. (2019), recovered from core P900 in the Arabian Sea; c: Elling et al., (2021), recovered from ODP sites 964 in the Ionian Sean and 967 in the Levantine basin.

		$\delta^{13}C$ values [‰ V-PDB]							
Sample	Age (cal ka BP)	BHT-34*S*	s.d.	BHT-*x*	s.d.	BHT-34*R*	s.d.	TOC	s.d.
Ca. Scalindua	–	−71.8	0.2	−73.7	0.4	n.d.*	–	–	–
Ca. Brocadia	–	−63.1	0.3	n.d.	–	−62.7	0.1	–	–
PE406-E1, S1	7.8	−24.7	0.4	−41.5	0.9	n.d.	–	−20.7	<0.1
PE406-E1, S1	8.9	−24.1	1.0	−42.7	0.8	n.d.	–	−21.7	<0.1
PE406-E1, S1	9.7	−24.5	0.3	−38.9	0.2	n.d.	–	−22.0	0.2
PE406-E1, non-sapropel	45.3	−22.6	0.4	n.d.	–	−32.8	0.7	−17.2	0.1
PE406-E1, 'S2'	51.3	−25.1	0.3	n.d.	–	−43.0	1.2	−17.2	<0.1
PE406-E1, 'S2'	52.2	−24.7	0.5	n.d.	–	−41.2	0.9	−17.3	0.2
PE406-E1, 'S2'	52.6	−25.3	1.3	n.d.	–	−41.5	0.6	−17.5	0.3
PE406-E1, non-sapropel	62.6	−23.5	0.3	n.r. **	>2.0	−33.6	1.5	−17.2	0.2
PE406-E1, non-sapropel	65.2	−22.2	0.3	n.d.	–	n.d.	–	−17.3	0.1
PE406-E1[a]	–	−24.1	1.1	−41.5	1.9	−41.2	4.8	−18.7	2.1
P900[b]	–	−26.6	1.4	−46.1	3.4	–	–	−20.9	0.8
ODP 964 and 967[c]	–	−27.2	1.1	−47.1	2.1	–	–	−22.0	1.5

* n.d.: not detected.
** n.r.: not reproducible (when the s.d. of measurements is >2.0).

atmospheric pressure chemical ionization (APCI) probe (Thermo Fischer Scientific, Waltham, MA), as previously described by van Kemenade et al., (2022). Separation was realized with a ZORBAX Eclipse XDB C18 column (Agilent, 3.0 × 250 mm, 5 μm), using MeOH as an eluant at 0.4 mL min^{-1}. Target lipids were detected using a positive ion monitoring of *m/z* 225–380 (140,000 ppm resolution), followed by a data dependent MS^2 (isolation window 1 *m/z*; resolution 17,500 ppm at *m/z* 200) of the 10 most abundant ions. The stepped normalized collision energy was set at 15, 22.5, 30. Mass chromatograms of the protonated molecules were used to integrate C_{18}[3]-, C_{18}[5]-, C_{20}[3]- and C_{20}[5]-ladderane FAMEs (*m/z* 291.232, 289.216, 319.263, 317.248, respectively), reported within 5 ppm mass accuracy. Quantification was performed using external calibration curves of isolated of C_{20}[3]- and [5] ladderane FAMEs standards (Hopmans et al., 2006). Concentrations are reported in accumulation rates (ng^{-1} cm^{-2} kyr^{-1}; supplementary material 1 Table S7). Identification of ladderanes was achieved by comparing retention times and spectra with in-house isolated C_{20}[3]- and [5] ladderane FAME standards (supplementary material 2, Fig. S3) and with C_{18}[3]-, C_{18}[5]-, C_{20}[3]- and C_{20}[5]-ladderane FAMEs in a biomass sample of *Ca.* Kuenenia (Rattray et al., 2008). Additionally, although PUFAs were removed during the sample preparation (see Section 2.4.2), commercially available C_{18}:3- and C_{20}:3-polyunsaturated fatty acids (PUFAs; Reagecon Diagnostics Ltd.; *m/z* 291.232 and 319.263) were derivatized and analyzed using the same method to assess potential interference with the identification of the ladderane FAMEs of the same *m/z*. The PUFA standards differed significantly in retention time (supplementary material 2, Fig. S4).

2.4.6. $\delta^{13}C$ analysis of BHT stereoisomers

Compound specific stable isotope analysis of $\delta^{13}C$ values of the BHT stereoisomers ($\delta^{13}C_{BHT\text{-}34S}$, $\delta^{13}C_{BHT\text{-}x}$, $\delta^{13}C_{BHT\text{-}34R}$) was performed on a GC-C-irMS system (Trace 1310 GC coupled to a Delta V MS via an GC Isolink II and Conflo IV, ThermoSceintific), equipped with a CP Sil-5 column (25 m length, 0.32 mm OD and 0.12 μm film thickness; Agilent,). Helium was used as a carrier gas with a flow rate of 2 mL min^{-1}. The programmed temperature was set at 70 °C and followed the next program: 20 °C min^{-1} to 130 °C, 10 °C min^{-1} to 190 °C and 1 °C min^{-1} to 320 °C where it remained for 10 min. Monitoring CO_2 gas with a predetermined stable carbon isotope value was measured at the beginning and end of each run to be able to assign isotope values to the compounds of interest. Performance of the entire system including the combustion interface was monitored using an in-house mixture of C_{20} and C_{24} perdeuterated *n*-alkane standards (IAEA) (STD < 0.5%). The isotopic composition of the acetyl group used in the acetylation of the BHT stereoisomers was determined by acetylation of *myo*-inositol with a predetermined stable carbon isotope value, which was then subtracted from the $\delta^{13}C$ BHT values, using a mass balance correction. Isotopic compositions are reported relative to the VPDB standard for C.

3. Results

3.1. Total organic carbon and total nitrogen

Throughout the record, sedimentary bulk total organic carbon (TOC) content ranges from 0.2 to 2.8%, showing a $\delta^{13}C$ value ($\delta^{13}C_{TOC}$) of −16.5 to −22.7‰ (Fig. 3b). Total nitrogen (TN) content ranges from 0.02 to 0.20%, with $\delta^{15}N$ values ($\delta^{15}N_{TN}$) of 0.9–5.0‰. TOC and TN content are relatively stable in the time interval between 67.8 and 11.3 cal ka BP (TOC: 0.2–0.3%; TN: 0.02–0.03%), while $\delta^{13}C_{TOC}$ and $\delta^{15}N_{TN}$ values range from −20.1 to −16.5‰ and from 4.0 to 5.9‰, respectively (Fig. 3b). Between 10.4–8.1 cal ka BP, TOC and TN are relatively elevated (TOC: 0.9–2.8%; TN: 0.10–0.20%), while $\delta^{13}C_{TOC}$ and $\delta^{15}N_{TN}$ values are lower ($\delta^{13}C_{TOC}$: −22.7 to −20.4%; $\delta^{15}N_{TN}$: 0.9–2.2‰). Maximum TOC and TN content and minimum $\delta^{13}C_{TOC}$ and $\delta^{15}N_{TN}$ values are observed at 9.4 cal ka BP. Between 7.8–1.4 cal ka BP, TOC is 0.2–0.4% ($\delta^{13}C_{TOC}$: −20.7 to −18.7%) and TN is 0.02–0.05% ($\delta^{15}N_{TN}$: 3.9–5.6%).

3.2. Lipid biomarkers

3.2.1. Bacteriohopanetetrols

Unsaturated BHT-CE was not detected in this study. BHT-34*S* was present throughout the sedimentary record, with accumulation rates (ARs) ranging between 6.7 × 10^6–7.0 × 10^9 ru g^{-1} cm^{-2} kyr^{-1} (supplementary material 1, Table 2). BHT-*x* (Fig. 4a) was present in sediments from 67.8 to 53.9 and 49.2 to 1.4 cal ka BP (except at 42.9 cal ka BP), at ARs between 2.6 × 10^7–5.6 × 10^9 ru g^{-1} cm^{-2} kyr^{-1} (BHT-*x* ratio: 0.03–0.59). BHT-*x* ARs peaked (in relation to background values) between 9.7–5.4 cal ka BP. BHT-34*R* stereoisomer was detected in sediments between 67.8–56.6 cal ka BP (Fig. 4a), with values of 1.0 × 10^7–5.0 × 10^8 ru g^{-1} cm^{-2} kyr^{-1} (BHT-34*R* ratio [3]: 0.02–0.68) and between 54.3–42.9 cal ka BP (except at 53.9 cal ka BP), with values of 4.0 × 10^6–1.1 × 10^9 ru g^{-1} cm^{-2} kyr^{-1} (BHT-34*R* ratio: 0.02–0.76).

In the nine sediment horizons selected for compound-specific $\delta^{13}C$ stable isotope analysis of the BHT stereoisomers (Table 1), $\delta^{13}C_{BHT\text{-}34S}$ values range from −25.3 to −22.2‰ (median, 'MD': −24.1 ± 1.1‰). In the three horizons recovered from the S1 time interval (7.8, 8.9 and 9.7 cal ka BP), $\delta^{13}C_{BHT\text{-}x}$ values range from −42.7 to −38.9‰ (MD: −41.5 ± 4.8‰). In the three horizons recovered from the 'S2' time interval (51.3, 52.2, 52.6 cal ka BP), $\delta^{13}C_{BHT\text{-}34R}$ values range from −43.0 to −41.2‰. At 45.3 and 62.6 cal ka BP, $\delta^{13}C_{BHT\text{-}34R}$ was −32.8 and −33.6‰, respectively ($\delta^{13}C_{BHT\text{-}34R}$ MD: −41.2 ± 1.9‰ for all five horizons). At 65.2 cal ka BP, BHT-34*R* concentrations were insufficient for $\delta^{13}C_{BHT\text{-}34R}$ analysis. $\delta^{13}C_{BHT}$ values were also determined in a *Ca.* Scalindua spp. and *Ca.* Brocadia spp. biomass enrichment culture, with the former showing values of −71.8‰ for $\delta^{13}C_{BHT\text{-}34S}$ and −73.7‰ for $\delta^{13}C_{BHT\text{-}x}$, and the latter showing values of −63.1‰ for $\delta^{13}C_{BHT\text{-}34S}$ and −62.7‰ for $\delta^{13}C_{BHT\text{-}x}$.

3.2.2. Ladderane fatty acids

Identified ladderane fatty acids were C_{18}[5]-, C_{20}[3]- and C_{20}[5]-ladderanes (concentrations reported in supplementary material 2, Table 3). Throughout the record, summed ladderane FA concentrations (Fig. 4c) were 0–2.4 ng^{-1} cm^{-2} kyr^{-1}, with higher concentrations observed between 62.6–42.9 cal ka BP (maximum at 53.9–53.0 cal ka BP) and between 9.1–6.5 cal ka BP (maximum at 7.8–7.3 cal ka BP). C_{18}[5]-ladderanes were solely detected in the younger sediments, at 9.1 cal ka BP (0.3 ng^{-1} cm^{-2} kyr^{-1}) and between 8.3–7.0 cal ka BP (0.1–1.1 ng^{-1} cm^{-2} kyr^{-1}). C_{20}[3]- and C_{20}[5]-ladderanes were detected in sediments between 62.6–42.9 cal ka BP, except at 55.2 and 54.8 cal ka BP sediments, both at ARs of 0.1–0.3 ng^{-1} cm^{-2} kyr^{-1}. The C_{20}[3]-ladderane was additionally present at 33.3 cal ka BP sediments (0.3 ng^{-1} cm^{-2} kyr^{-1}). The C_{20}[3]- and C_{20}[5]-ladderane ARs in the younger sediments (9.1–6.5 cal ka BP) were 0.3–1.2 ng^{-1} cm^{-2} kyr^{-1} (maximum at 9.1 cal ka BP) and 0.2–2.2 ng^{-1} cm^{-2} kyr^{-1} (maximum at 8.9 cal ka BP), respectively.

3.2.3. Heterocyte glycolipids

Identified heterocyte glycolipids were: C_5 HG_{30} triol, C_6 HG_{26} diol, C_6 HG_{28} diol and C_6 HG_{30} triol (concentrations reported in supplementary material 2, Table 4). The C_5 HG_{30} triol (Fig. 4d) was present in sediments from 11.3 to 5.4 cal ka BP (except at 7.5 and 6.5 cal ka BP) at ARs of 1.0 × 10^7–5.6 × 10^9 ru g^{-1} cm^{-2} kyr^{-1} (max. at 8.6 cal ka BP). C_6 HGs were detected in sediments from 62.6 to 50.9 cal ka BP (except at 53.1 and 53.0 cal ka BP) with ARs of 8.7 × 10^6–1.2 × 10^8 ru g^{-1} cm^{-2} kyr^{-1} (max. at 56.2 cal ka BP) and in sediments from 11.3 to 1.4 cal ka BP (except at 7.0 cal ka BP), at ARs of 2.2 × 10^7–3.7 × 10^9 ru g^{-1} cm^{-2} kyr^{-1} (max. at 8.6 cal ka BP). C_6 HGs are reported as their summed abundance (Fig. 4d): they were detected in sediments of 47.5, 34.2 and 33.3 cal ka BP with ARs of 8.3 × 10^6, 2.0 × 10^7 and 4.2 × 10^7 ru g^{-1} cm^{-2} kyr^{-1}, respectively.

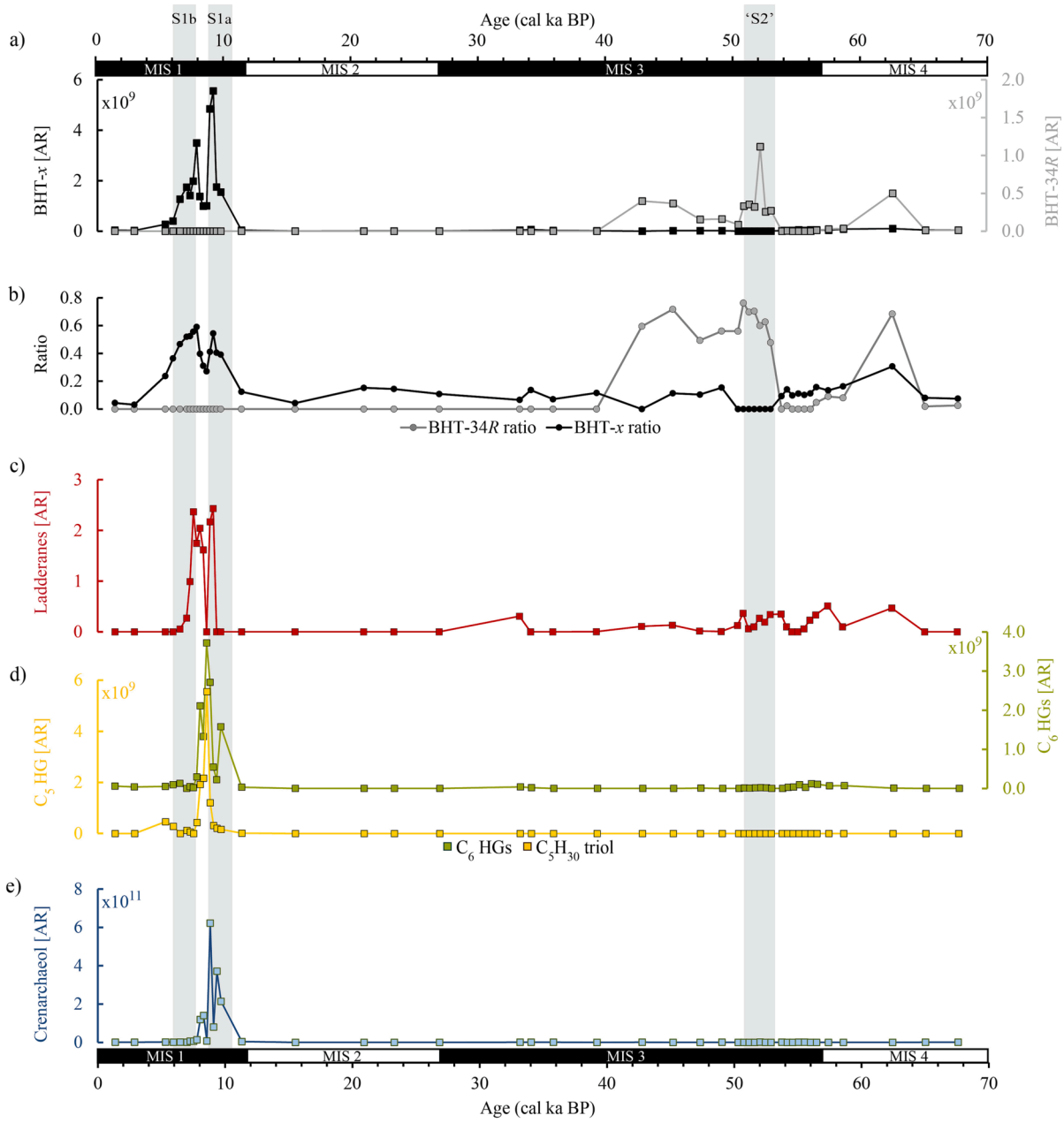

Fig. 4. Lipid biomarker accumulation rates (ARs) at site 64PE406-E1: a) bacteriohopanetetrol (BHT)-*x* and BHT-34*R* [ru g^{-1} cm^{-2} kyr^{-1}]; b) BHT-34*R* ratio in grey and BHT-*x* ratio in black; c) summed C_{18}[3]-, C_{18}[5]-, C_{20}[3]- and C_{20}[5]-ladderane FAs [ng^{-1} cm^{-2} kyr^{-1}]; d) Heterocyte glycolipids (HGs) with summed C_6 HGs (C_6 HG_{26} diol, C_6 HG_{28} diol and C_6 HG_{30} triol) plotted on the right y-axis and C_5 HG_{30} triol plotted on the left y-axis [ru g^{-1} cm^{-2} kyr^{-1}]; and e) crenarchaeol [ru g^{-1} cm^{-2} kyr^{-1}]. Timing of S1a, S1b (Rohling et al., 2015; Grant et al., 2016) and 'S2' (Muerdter et al., 1984), are shown in grey. Glacial and interglacial marine isotope stages are indicated in white and black, respectively.

3.2.4. *Crenarchaeol*

Crenarchaeol was detected throughout the sedimentary record at ARs of 2.4×10^7–6.2×10^{11} ru g^{-1} cm^{-2} kyr^{-1} (Fig. 4e; supplementary material S2, Table 5), with peak ARs at 9.7 to 7.8 cal ka BP (7.1×10^9–6.2×10^{11} ru g^{-1} cm^{-2} kyr^{-1}; max. at 8.9 cal ka BP).

3.3. *Benthic foraminiferal bottom water oxygenation index*

Low oxygen indicator species (LOS) varied throughout the core in abundances of 0–8%, relative to the total number of benthic foraminifers (supplementary material 1 and 2, Fig. S5 and Table 6, respectively). Based on the LOS cumulative percentage and the absence of foraminifera (where the BWO index was set to 0), the benthic foraminiferal BWO index was determined for the entire record (Fig. 3c), with values ranging between 0.0 (i.e., anoxic bottom waters) and 1.0 (i.e., fully oxygenated bottom waters). Through most of the record, the BWO index indicates fully oxygenated conditions (BWO ~1) with the exception of two periods: i) during 'S2', the BWO index shows a decrease (reaching 0.6) indicating oxygen depleted waters without reaching anoxia, ii) at 11.3 cal ka BP the BWO index was 0.9 and decreased to 0 during S1. During S1, the BWO index was 0 between 10.4–8.8 and 7.8–7.5 cal ka BP, with the amount of total foraminiferal counts <4, indicating anoxic bottom water conditions. At 8.8 to 8.0 cal ka BP (between S1a and S1b), an interval was observed where the BWO index was 1.0.

4. Discussion

EMS sapropels, characteristic of basin-wide deoxygenation events,

are valuable for the investigation of past marine nitrogen cycling under low oxygen conditions. In the following sections, lipid biomarkers of microorganisms involved in the nitrogen cycle are analysed with redox sensitive trace metals and benthic foraminifer assemblages to constrain past nitrogen cycling activities and redox conditions during the Holocene sapropel S1 (~10.5–6.1 ka BP; Section 4.1) and the 'S2' event of the late Pleistocene (53–51 ka BP; Section 4.2). Ultimately, by assessing the shifts in the N-cycle occurring during the different depositional environments of S1 and 'S2', further insights can be obtained on feedback mechanisms between the nitrogen cycle and water column deoxygenation (Section 4.3).

4.1. Nitrogen cycling dynamics under altering redox conditions during deposition of the Holocene sapropel S1

4.1.1. Loss of fixed N throughout the S1 event

The presence of anammox biomarkers indicate loss of bioavailable N via marine anammox bacteria (*Ca.* Scalindua spp.) throughout S1 deposition (Fig. 4a, c). The BHT-*x* ratio [1] reflects the relative contribution of BHT-*x* synthesized by the anaerobe *Ca.* Scalindua spp. (Rush et al., 2014; Schwartz-Narbonne et al., 2020; van Kemenade et al., 2022), over the total BHT-34*S* pool, ubiquitously synthesized by mostly aerobic bacteria. From 9.7 cal ka BP onwards, the BHT-*x* ratio is >0.2 (Fig. 4b), suggesting a dominant presence of *Ca.* Scalindua spp. within the total pool of BHT-34*S* synthesizing bacteria (van Kemenade et al., 2022). Ladderane FA and BHT-*x* ARs further suggest *Ca.* Scalindua spp. was most abundant at ~9.1 cal ka BP (Fig. 4a, c).

At the onset of S1a (~10.5 cal ka BP), the abrupt disappearance of benthic foraminifera reflects a quick establishment of anoxic bottom waters at site 64PE406-E1. The depth at the core location (1760 mbss) is at the edge of the stagnant and euxinic deep-water (DW) during S1 (<1800 mbss; De Lange et al., 2008) and anoxic intermediate water, which were more frequently ventilated (sapropel intermediate water; SIW; ~500–1800 mbss; Zirks et al., 2019). During S1, SIW is believed to have flowed from the Aegean Sea towards the Levantine basin, becoming progressively depleted in oxygen in response to the increased remineralization of the sinking OM (Zirks et al., 2019; 2021). Indeed, the Ba/Al profile (Fig. 3e) points to increased export productivity between ~10.5–6.1 cal kyr BP, typically thought to be a response to enhanced Nile River discharge (see review Rohling et al., 2015), recorded from ~11.3 cal ka BP onwards (Hennekam et al., 2014; 2015; Weldeab et al., 2014). Mild DW euxinia is also recorded during S1a (Azrieli-Tal et al., 2014; Andersen et al., 2020). This is thought to be the result of a slowdown of the Mediterranean thermohaline overturning system, resulting in a cessation of DW renewal (*e.g.*, Sarmiento et al., 1988; de Lange et al., 2008). As our site is located at the boundary of the anoxic non-euxinic SIW (Matthews et al., 2017; Zirks et al., 2019) and euxinic DW, the concurrent increase in Mo and U (Fig. 3e), indicative of euxinic conditions (Tribovillard et al., 2006; Algeo and Liu 2020), likely reflects a euxinic sediment–water interface, and possibly euxinic bottom waters. As anammox bacteria are inhibited by the presence of free sulfide (Jensen et al., 2008), *Ca.* Scalindua spp. likely occupied a niche in the anoxic SIW, but not in the euxinic DW or sediments. Hence, the more progressive oxygen-depletion of the SIW may have resulted in a gradual expansion of anammox into the SIW, causing maximum anammox to occur with a lag (of ~1.4 kyr) after the onset of bottom water anoxia.

A dip in anammox biomarkers is observed at ~8.6 cal ka BP. At this time, the BWO index records a return of oxygenated bottom water conditions (~8.6–8.1 cal ka BP; Fig. 3c). This oxygenation period (8.5–8.0 cal ka BP; Grant et al., 2016) relates to the well-known S1 interruption, corresponding to the re-ventilation of the EMS, which may be associated to the 8.2 ka BP global cooling event (Rohling et al., 1997). Likely, the return of more oxygenated SIW (Zirks et al., 2021) led to a crash of *Ca.* Scalindua spp. population in the water column. However, after 8.3 cal ka BP, anammox biomarker ARs increase again. While the anammox process is inhibited by oxygen concentrations as low as 1 μM (Strous et al., 1997), in the marine environment *Ca.* Scalindua spp., are known to inhabit anoxic micro-niches, allowing them to thrive at ambient oxygen concentrations up to ~20 μM (Woebken et al., 2007). In addition, evidence for anammox bacterial presence has been detected in marine environments with oxygen levels up to ~9–50 μM (Kuypers et al., 2005; Hamersley et al., 2007; Jensen et al., 2008; Kalvelage et al., 2011; Hamasaki et al., 2018; van Kemenade et al., 2022). (Pore) waters in the Levantine basin during the S1 interruption must thus have been sufficiently oxygen-deficient (at least < 50 μM; van Kemenade et al., 2022) to provide a suitable niche for *Ca.* Scalindua spp.

A progressive down-ward moving oxidation front has affected the composition of the upper part of the original S1b layer. Previously described discrepancies between the TOC and Ba/Al profiles (Thomson et al., 1995; van Santvoort et al., 1996; de Lange et al., 2008), in which the latter is thought to reflect the original primary productivity, and hence C-deposition signal, is indicative of the post-depositional oxidation ('burn-down') of sapropels. Burn-down of the upper part of S1 at our site occurred from ~7.8 cal ka BP onwards (Fig. 3b, d). The lower Mn/Al peak (start at ~7.8 cal ka BP; Fig. 3d) is thought to mark the depth of the currently active oxidation front (Higgs et al., 1994; Thomson et al., 1995; van Santvoort et al., 1996), as Mn precipitates under oxygenated conditions (Tribovillard et al., 2006). The upper Mn/Al peak (start at ~6.1. ka BP; Fig. 3d) is thought to mark the time of re-introduction of oxygenated bottom waters at the end of S1, as a response to the resumption of DW formation (Filippidi and de Lange et al., 2019). The BWO index is thought to largely withstand post-depositional diagenesis (Jorissen et al., 2007). A near-absence of benthic foraminifera shows anoxic conditions between 7.8–7.5 cal ka BP, and their re-occurrence the establishment of fully oxygenated conditions from ~6.5 cal ka BP onwards (Fig. 3c).

This post-depositional oxidation likely also affected biomarker concentrations (Sinninghe Damsté et al., 2002a), suggesting the original ARs of anammox biomarkers in the oxidized section of S1b must have been higher than reported here. Despite this, ladderane ARs in S1b still surpass those of S1a, suggesting that loss of bioavailable N via anammox was probably more intense during S1b than during S1a. This is supported by the observation that anammox biomarker concentrations normalized against TOC (which should retain the original signal better as both TOC and lipids are sensitive to oxic degradation) are also higher in S1b than in S1a (supplementary material 1, Fig. S2). Unexpectedly, however, while ladderane lipids undergo β-oxidation under the influence of low amounts (<3 uM) of oxygen, their corresponding short-chain (SC) degradation products (SC-ladderanes; Rush et al., 2011; 2012), were not detected in the oxidized section of S1b, nor in the rest of the record.

The BHT-*x* ratio (which is likely not affected by diagenesis) is substantially elevated (>0.2) across the S1 interruption and during S1b, showcasing a similar relative abundance of *Ca.* Scalindua spp. in the total bacterial pool as during S1a (Fig. 4b). In the contemporary Benguela oxygen minimum zone, where similar BHT-*x* ratio values have been observed as in S1 (>0.2; van Kemenade et al., 2022), the total amount of N loss via anammox was estimated to be 1 Tg N yr^{-1} (Kuypers et al., 2005). Accordingly, loss of bioavailable N via anammox is thought to have been substantial from ~9.1 cal ka BP (~1.4 kyr after the onset of anoxia) until the end of the S1 event.

4.1.2. N_2-fixation during S1a and S1 interruption

Hexose HG ARs are elevated across S1a (from 9.6 cal ka BP onwards), and during the S1 interruption, with peak values at 8.6 cal ka BP (Fig. 4d). The C_6 HG_{26} diol, C_6 HG_{28} diol and C_6 HG_{30} triol observed in this study are biomarkers for freshwater/brackish cyanobacteria of the order Nostocales (Bauersachs et al, 2009; Wörmer et al., 2012). The presence of C_6 HGs in sapropel S5 has been attributed to the presence of a brackish surface layer formed because of enhanced Nile outflow into the EMS (Bale et al., 2019). The presence of C_6 HGs in S1 suggests that, at least occasionally, the surface waters must have been sufficiently

brackish to provide a suitable niche for Nostocales cyanobacteria. Indeed, maximum intensities of Nile River discharge into the EMS occur around 9.5 ka BP and gradually decrease after the S1 interval, from 6.5 cal kyr onwards (Hennekam et al., 2014; 2015; Weldeab et al., 2014). Modern Nile floods are known to reduce salinity in the EMS basin. The much larger flooding occurring during S1a (Woodward et al., 2022) could have resulted in the brackish water conditions inferred from this study.

A peak in C_5 HG_{30} triol is observed in the S1 interval, slightly surpassing C_6 HG ARs (factor 1.5; Fig. 4d). C_5 HGs are synthesized by marine DDAs, with the C_5 HG_{30} triol being specifically associated with the heterocytous cyanobacterium *Richelia intracellularis* (Schouten et al., 2013; Bale et al., 2015). Its corresponding host diatom, *Hemiaulus hauckii*, has previously been reported to occur in sapropel S5 sediments (Kemp et al., 1999). Potentially, C_6 HG-producing Nostocales inhabited the upper photic zone, where conditions were likely fresher, while C_5 HG derived from DDAs may have inhabited the lower photic zone, where conditions were more saline compared to the brackish surface waters. Alternatively, intermittent periods with brackish surface layer conditions, favoring Nostocales, could have alternated with more saline conditions that favored DDAs. During S1b, C_6 HGs and the C_5 HG remain present at background levels, with a slight elevation of the C_5 HG at 6.0 to 5.3 cal ka BP, possibly reflecting the return of more saline conditions in surface waters after the re-ventilation of the EMS that occurred after sapropel deposition (*e.g.*, de Lange et al., 2008).

No biomarker evidence for the occurrence of the filamentous cyanobacterium *Trichodesmium* spp. (unsaturated BHT-CE; Talbot et al., 2008) was detected. Potentially, low amounts of unsaturated BHT-CE might have remained below the detection level of our method, as *Trichodesmium* spp. has been found to occur in low abundances in the contemporary Mediterranean (Yogev et al., 2011). Even so, *Trichodesmium* spp. are known to be outcompeted by DDAs at higher phosphorus and iron levels (Follett et al., 2018). Hence, no substantial N_2-fixation by *Trichodesmiun* spp. is thought to have taken place during S1.

In the modern EMS, $\delta^{15}N$ values of suspended particulate matter ($\delta^{15}N$ of −0.2‰; Pantoja et al., 2002) are similar to those observed in S1 sediments (Fig. 3b), while the surface sediments are similarly enriched (>5‰; Fig. 3b) as non-sapropel sediments (Sachs and Repeta, 1999). This resulted in the hypothesis that N_2-fixation during sapropel deposition is similar to the present-day EMS (Sachs and Repeta, 1999), and that elevated $\delta^{15}N$ levels in non-sapropel sediments reflect diagenetic isotope enrichment (Sachs and Repeta, 1999; Möbius et al., 2010). Later, Higgins et al. (2010) showed that the offset between $\delta^{15}N$ values found in chlorins and in total N is 5‰ in both sapropel and non-sapropel sediments (reflecting isotopic fractionation during chlorophyll biosynthesis by eukaryotes; Higgins et al., 2011), indicating that $\delta^{15}N_{TN}$ values reflect the original biomass, and not diagenetic isotopic alteration.

Modern-day N_2-fixation rates are, however, low (Yogev et al., 2011) and do not explain the depleted $\delta^{15}N$ values observed in the water column and surface sediments. These low rates are thought to be caused by the extremely low bioavailability of phosphorus (P), whereas iron (Fe) is not considered a limiting factor (Ridame et al., 2011). Mara et al., (2009) showed that the depleted $\delta^{15}N$ values observed in the modern EMS result from atmospheric deposition of exogenous aerosol N ($\delta^{15}N$ of −3.1‰). The influx of reactive N species (*e.g.*, via atmospheric deposition and rivers) is thought to account for >50% of total bioavailable N in the modern EMS (Krom et al., 2004).

A different mechanism seems to have occurred during sapropel deposition. Discrepancies between the HG (max. at 8.6 cal ka BP) and TOC profile (max. at 9.4 cal ka BP), indicate that increases in the concentrations of HGs during S1 are not simply a preservation signal. This provides evidence for enhanced N_2-fixation by heterocyte cyanobacteria during especially the later S1a stages and the S1 interruption, in comparison to non-sapropel sediments and S1b. At maximum Nile flooding (~9.5 cal ka BP; Hennekam et al., 2014), increased Nile input led to increased P influx as dissolved, particulate, reactive and detrital P (Slomp et al., 2002; Zirks et al., 2021). Deposition of organic- and iron bound-P and subsequent release under anoxic conditions is thought to have resulted in the enhanced availability of reactive P species in SIW (500–1800 m), which could be recycled into shallower waters (200–500 m; Zirks et al., 2021). In turn, turbulent mixing of the surface and intermediate waters is thought to lead to a dispersal of N and P (van Capellen et al., 2014). Less intense P-release occurs after the 8.2 ka BP ventilation event, as pre-sapropelic oligotrophic conditions slowly returned (Zirks et al., 2021). P-recycling into intermediate water depths may have favored DDAs in the later S1a stages and during the S1 interruption. In addition, loss of bioavailable N via anammox may have promoted growth of diazotrophs over other primary producers (Kuypers et al., 2004). *Ca.* Scalindua spp. are typically most abundant at the secondary nitrite maximum, below the oxycline (Rush et al., 2012). This implies that the most extensive N-loss likely occurred at the upper margin of the anoxic SIW, which may have affected N-availability in the euphotic zone.

4.1.3. Aerobic ammonium oxidation by Thaumarchaeota

The AR of crenarchaeol, uniquely synthesized by autotrophic aerobic ammonium oxidizing archaea (AOA) Thaumarchaeota (Sinninghe Damsté et al., 2002b) is substantially elevated across S1a (Fig. 4e). Nonetheless, crenarchaeol is detected throughout the record showing a continuous presence of Thaumarchaeota. As such, it is possible that the elevated crenarchaeol accumulation rates during S1a reflect enhanced preservation under anoxic conditions, rather than an increase in the abundance of Thaumarchaeota. Lower crenarchaeol ARs in non-sapropel sediments may simply be the result of oxygen exposure (Sinninghe Damsté et al., 2002a). However, crenarchaeol concentrations normalized to TOC (supplementary material 1 Fig. S2), also show increased crenarchaeol from 11.3 cal ka BP, with a peak at 8.9 cal ka BP. A similar S1 trend in crenarchaeol concentration was observed by Castañeda et al. (2010). These authors proposed that the increase in NH_4^+ oxidation was a response to enhanced supply of high-nutrient freshwater discharge into the Levantine basin. Indeed, our observed elevated crenarchaeol concentrations are congruent with a recorded increase in river discharge from 11.5 ka BP onwards, remaining high until 6.5 ka BP (Hennekam et al., 2014; 2015; Weldeab et al., 2014). Crenarchaeol remains present throughout the S1 interruption and S1b, but with markedly lower ARs. Reduced nutrient-influx and remineralization rates in these later S1 stages may have limited NH_4^+ supply, and hence, Thaumarcheota.

Potentially, the increase in Thaumarcheotal abundance may have contributed to providing anammox bacteria with the necessary NO_2^- to perform the anammox reaction. In the Black Sea euxinic basin, AOA and ammonium oxidizing bacteria (AOB) have been suggested to provide up to 40% of the NO_2^- for anammox bacteria (Lam et al., 2007). As anammox bacteria are inhibited by the presence of free sulfide (Jensen et al., 2008), the *Ca.* Scalindua spp. population in the Black Sea is located right above the sulfidic-anoxic boundary (at ca. 110 mbss). Here, they co-inhabit the suboxic-anoxic zone with Thaumarchaeota (Lam et al., 2007). A similar niche-partitioning likely occurred during sapropel S5, where anammox bacteria inhabited the upper water column, due to the occurrence of photic zone euxinia (Rush et al., 2019). In contrast, in the Arabian Sea, Thaumarchaeota inhabit the upper suboxic chemocline and anammox bacteria the lower anoxic chemocline (Pitcher et al., 2011). The large depth segregation of anammox bacterial and Thaumarcheotal niches (>400 m) is thought to indicate that no direct coupling of their metabolism, nor competition for substrates, takes place.

Ca. Scalindua spp. can be found over a much larger O_2 range than previously assumed (<50; Woebken et al., 2007; Hamasaki et al., 2018; van Kemenade et al., 2022), being mainly limited by NO_2^- availability (Rush et al., 2012). More recently, oxygen assays showed that anammox and aerobic nitrifying bacteria share a large overlapping range in O_2 concentrations (>0–20 μmol/L; Kalvelage et al., 2011). Hence, we propose *Ca.* Scalindua spp. likely inhabited the upper SIW, at the depth

of the secondary nitrite maximum where Thaumarchaeota (and potentially also aerobic nitrifiers) may have provided the necessary NO_2^- for the anammox process. Also, as anammox bacteria are known to have an extremely high affinity for NH_4^+ (<1 μM; Strous et al., 1999), competition for NH_4^+ with Thaumarchaeota was possibly limited.

4.2. N-cycling during the Late Pleistocene (~70–11 cal ka BP), including 'S2' deposition (~55–52 cal ka BP)

4.2.1. Lipid biomarker evidence for the occurrence of anammox bacteria during MIS 3/4

Elevated ladderane FAs (in relation to background values) between ~63–56 (MIS 3/4), 54–39 (MIS 3), and at 34 cal ka BP (MIS 3) show the increased presence of anaerobic ammonium oxidizing bacteria over these time intervals. However, no corresponding BHT-*x* elevations, as observed for S1, are observed. Curiously, the BHT-34*R* stereoisomer was detected at 67.8–56.6 and 54.3–42.9 cal ka BP (Fig. 4b). BHT-34R is known to be synthesized by freshwater/brackish anammox bacteria *Ca.* Brocadia spp., (Schwartz-Narbonne et al., 2020), but also by species of acetic acid bacteria (Peiseler and Rohmer, 1992), the aerobic terrestrial nitrogen-fixing bacteria *Frankia* spp. (Rosa-Putra et al., 2001) and the aerobic methanotrophic bacterium *Methylocella palustris* (van Winden et al. 2012). While BHT-*x* does not show a significant correlation with the ladderane FA distribution in the MIS 2–4 sediments, BHT-34R does ($\rho < 0.05$).

To further explore the source organism of the detected BHT-34*R*, compound specific $\delta^{13}C$ measurements were conducted. Median $\delta^{13}C_{BHT\text{-}x}$ and $\delta^{13}C_{BHT\text{-}34R}$ values were −41.5‰ (±1.9‰) and −41.2‰ (±4.8‰), respectively (Table 1). $\delta^{13}C_{BHT\text{-}34R}$ values are close to expected values, if anammox bacteria were the source organisms, given the stable carbon isotope fractionation effect with which *Ca.* Brocadia spp. synthesizes BHT-34*R* ($^{13}\varepsilon_{CO2(aq)\text{-}BHT\text{-}34R}$: ca. −36.3‰ at a temperature of 35 °C; Schouten et al., 2004) when assuming dissolved carbon dioxide (DIC) was +1 (modern EMS; Rohling et al., 2015) to 4‰ (reconstructed value during sapropel deposits; Elling et al., 2021). Also, the equally depleted $\delta^{13}C$ values of BHT-*x* and BHT-34*R* suggest a similar carbon fixation pathway, which in the case of *Ca.* Scalindua spp., is thought to be the acetyl-CoA pathway (Schouten et al., 2004; Strous et al., 2006; Kartal et al., 2013). Additionally, values recorded during 'S2' are similar (−43.0 to −41.2‰; Table 1) to those recorded for marine anammox bacteria in the Arabian Sea (Lengger et al., 2019) and the EMS (Hemingway et al., 2018; Elling et al., 2021). Potentially, relatively low $\delta^{13}C_{BHT\text{-}34R}$ values could also be synthesized by the methanotroph *M. palustris*. Yet, Type II methanotrophs do not have consistently $\delta^{13}C$-depleted lipids (Kool et al., 2014). Together with the co-occurrence of ladderane lipids, it is more likely that anammox is the source of the BHT-34*R* detected in 'S2'. Future work is nonetheless required to differentiate the $\delta^{13}C_{BHT\text{-}34R}$ values of the different producers.

So far, inventories of BHT stereoisomer synthesis by marine anammox bacteria have focused solely on pelagic *Ca.* Scalindua spp. (Rush et al., 2014; Schwartz-Narbonne et al., 2020; van Kemenade et al., 2022), and little is known on the synthesis by sedimentary marine anammox bacteria. Marine anammox candidate genus, *Ca.* Bathyanammoxibiaceae, was recently described in marine sediments and terrestrial environments (Zhao et al., 2022). *Ca.* Bathyanammoxibiaceae have been detected predominantly in the nitrite-ammonium transition zones of marine sediments (Zhao et al., 2022), which would likely also be the niche of anammox at site 64PE406-E1 during the intermittent periods of MIS3/4, where anammox biomarkers were detected. However, lipid characterization of *Ca.* Bathyanammoxibiaceae is required to determine whether this genus might synthesize BHT-34*R*.

Peaks in ladderane lipids coincide with minor fluctuations in the benthic foraminifera-derived BWO index. This would indicate intermittent bottom water deoxygenation during MIS3/4. The BWO index dips during MIS3/4, most perspicuous from 53.0 to 52.2 cal ka BP (Fig. 3c), are based on the increased relative abundance of the deep infaunal low-oxygen indicator taxon *Globobulimina* spp.. Reduced bottom water oxygen concentration may have culminated in anoxia at the sediment surface, allowing anammox.

When anoxic conditions are introduced, Mn^{2+} diffuses upwards and is either lost to the water column if bottom waters are anoxic, or precipitates as Mn oxides in the sediments if pore water oxygen is encountered (see review Tribovillard et al., 2006). Mn oxides are reductively removed when sedimentary redox conditions become anoxic again (*e.g.*, this type of post-depositional diagenesis likely occurred after the 'S2' interval), but the original signal may be preserved when dissolution provides enough Mn^{2+} for Mn-carbonate formation (Chiu et al., 2022). As such, the Mn/Al peak at 53 to 49 cal ka BP (Fig. 3d), likely suggests enhanced Mn cycling related to sedimentary anoxia occurred prior to 53 cal ka BP, and subsequent re-ventilation from 53 cal ka BP onwards.

The BWO index fluctuations, Mn/Al peak values and the occurrence of anammox biomarkers correspond to the timing reported for bottom water deoxygenation between 53–51 cal ka BP (attributed to the 'missing' S2 sapropel), associated with a reported weakening of the intermediate circulation in the Sicily channel, which in turn slowed intermediate water ventilation in the EMS (Di Donato et al., 2022). The weakening of the thermohaline circulation might have been a response to enhanced stratification due to an activation of North-African coastal wadis advected by Mediterranean storms during MIS3/4 (Blanchet et al., 2021). Possibly these short-lasting and less intense humid events during MIS3/4 (Blanchet et al., 2021), might not have been sufficient for complete development of bottom water anoxia, but still affected the biogeochemical cycling in the EMS. Only around ~55–52 cal ka BP (*i.e.*, the timing of 'S2'), the nutrient load may have been sufficient to allow an appreciable increase in productivity (as indicated by the minor Ba/Al elevation at this time; Fig. 3d), resulting in enhanced bottom water deoxygenation (as indicated by the BWO index and Mn profile). This may be caused by the only Nile flood recorded to occur at this time; Ducassou et al., (2008; 2009) detected clastic mud facies associated with Nile floods at ~55 cal ka BP in a record recovered from the Levantine basin (FKSO4). While the absence of persistent fully anoxic bottom waters means that 'S2' does not qualify as a (typical) sapropel, we hypothesize that the abovementioned short periods of water column deoxygenation resulted in an anoxic sediment–water interface that provided a niche for anammox bacteria.

4.2.2. No evidence for enhanced N_2-fixation and aerobic ammonium oxidation

C_6 HGs were present from 63 to 51, at 48, and from 34 to 33 cal ka BP (Fig. 4d), albeit with very low ARs, suggesting limited increases in the abundance of Nostocales occurred at these time periods (Schouten et al., 2013; Bale et al., 2015). C_5 HGs and unsaturated BHT-CE were not detected, indicating DDAs and *Trichodesmium* spp. were absent or too low in abundance for detection. Although crenarchaeol is detected throughout the 64PE406-E1 record, no elevation in relation to background levels is observed over 'S2' (Fig. 4e). The relatively low (in comparison with S1 sediments) HG and crenarchaeol ARs throughout the late Pleistocene, might indicate these lipids were degraded, as enhanced preservation was not warranted by bottom water anoxia (Sinninghe Damsté et al., 2002a). Nonetheless, HG and crenarchaeol concentrations normalized on TOC (supplementary material 1 Fig. S2) are also continuously low, remaining far below S1 levels. This likely suggests ammonium oxidation by Thaumarchaeota and N_2-fixation by DDAs was markedly more limited in the late Pleistocene, than during S1 deposition.

The EMS water column throughout most of MIS 2–4 seems to reflect modern oligotrophic conditions. In the modern EMS, Thaumarchaeota are known to also occur in the oxic mesopelagic waters (De Corte et al., 2009). Measured nitrification rates in the Mediterranean Sea are 72–144 nmols N l^{-1} d^{-1} (Bianchi et al., 1999). As such, ammonium oxidation by Thaumarchaeota is likely to have contributed significantly to N-

recycling throughout the late Pleistocene in the EMS. In contrast, only low rates of N_2-fixation ($\leq$0.5 nmols N l^{-1} d^{-1}; Ibello et al., 2010) have been measured in the modern Mediterranean Sea (Ibello et al., 2010; Yogev et al., 2011). Diazotrophs thus provide only a minor source of the bioavailable N. These low rates are likely caused by an extreme P depletion, resulting from an accumulation of N as anammox and denitrification seem not to occur in the modern EMS (Krom et al., 2010). Even so, at brief periods during MIS 3/4, the co-occurrence of C_6 HGs and anammox biomarkers might indicate that loss of bioavailable N via anammox (and potentially denitrification) drove N_2-fixation rates by heterocyte cyanobacteria at intermittent periods of bottom water deoxygenation (see Section 4.2.1).

4.3. Insights on feedbacks between the nitrogen cycle and anoxia, based on the S1a, S1b, and 'S2' deoxygenation events

Sapropel depositions record information on paleoclimatic and palaeoceanographic changes during anoxic events, linked to the orbital cycle of the Earth's precession (Rossignol-Strick, 1985; Hilgen, 1991). They are considered potential analogues for modern ocean deoxygenation (Mancini et al., 2023). Additionally, sapropels reveal sequences of biogeochemical processes in response to climate change, and have therefore been proposed as a more recent framework to assess Mesozoic anoxic events (Meyers and Negri, 2003). The S1 and 'S2' deoxygenation events of the EMS offer insights on biogeochemical feedbacks under different depositional conditions, which enables better constraints of biogeochemical models. Below we outline the proposed feedback modes between the N-cycle and marine (de)oxygenation during deposition of S1a, S1b and 'S2', which offer a framework for nitrogen cycling responses to changing redox conditions.

First of all, during the S1a deposit in the Levantine basin, a positive N-cycling feedback on anoxia is thought to occur. Based on modern-environmental distributions, *Ca.* Scalindua spp. is expected to predominantly inhabit the upper SIW at the depth of the secondary nitrite maximum. In the contemporary EMS, limited mixing is thought to occur between EMS intermediate (150–600 m) and deep water (>600 m) layers (Powley et al., 2016). Turbulent mixing of the surface and intermediate waters, however, is thought to lead to a dispersal of N and P (van Capellen et al., 2014). Increased *Ca.* Scalindua spp. abundance in the upper SIW could thus have led to N-limitation in the euphotic zone. During Cretaceous anoxic events, loss of bioavailable N via anammox and denitrification has been proposed to drive N_2-fixation rates, by providing diazotrophs with a competitive advantage over other primary producers (Kuypers et al., 2004). In the EMS, peak DDA abundance in S1 occur ~0.5 kyr after peak *Ca.* Scalindua spp., abundance (Fig. 4). Loss of bioavailable N via anammox may therefore have contributed to an increased presence of DDAs. The same mechanism was also proposed to occur in the Ionian Sea, where Elling et al. (2021) suggested that during S4, S5 and S74 sapropels, anammox promoted the occurrence of DDAs, which in turn sustained anoxia via enhanced degradation rates of the sinking OM. Furthermore, increased P availability during S1a in response to Blue Nile floods (Slomp et al., 2002; Zirks et al., 2021) may have favored the presence of DDAs over smaller-sized diazotrophs (Follett et al., 2018). Remineralization of the sinking DDAs would further promote anoxia in the SIW. In the Levantine basin, however, HGs derived from the smaller-sized Nostocales and larger-sized DDAs are more or less equally abundant (this study; Elling et al., 2021). Consequently, this would lead to a lower OM flux to the seafloor than in Ionian Sea sapropels, where HGs were solely sourced from DDAs (Elling et al., 2021). It must also be noted that the positive feedback of DDA abundance on anoxia was likely negligible compared to thermohaline circulation changes in response to the 8.2 ka BP global cooling event, which resulted in a re-ventilation and oxygenation of the EMS basin (Rohling et al., 2015).

Secondly, the decoupled peaks in abundance of cyanobacteria and anammox bacteria during S1b (*i.e.*, HG concentrations are relatively low, whereas anammox biomarker concentrations are as high as in S1a) shows that loss of bioavailable N was not sufficient to promote N_2-fixation by DDAs. We also propose that a return to more oligotrophic conditions during S1b, where P is no longer supplied in excess, limited the presence of DDAs at this time.

During the S2 interval, when Mn and benthic foraminifers indicate water column hypoxia and anoxic sediments, the intermittent deoxygenation events triggered enhanced N-loss via anammox (see Section 4.2). Yet, this N-loss during 'S2' did not trigger increased N_2-fixation via heterocyte cyanobacteria. This decoupling was probably caused by the large niche-segregation of anammox bacteria (proposed to inhabit the sediments at this time; see Section 4.2.1) and diazotrophs (in the euphotic zone). Also, the brief intervals of increased river runoff (Ducassou et al., 2008; 2009; Langgut et al., 2018; Blanchet et al., 2021) and the associated moderate water column deoxygenation (see Section 4.2.1) were likely not sufficient to provide the P (via riverine influx or a release of P from anoxic sediments) necessary to promote high DDA abundances. Under these more oligotrophic conditions, the negative feedback of the N-cycle on anoxia would likely have been stronger than the positive feedback.

Based on the results of this study, loss of bioavailable N via anammox can impose both i) negative feedback on anoxia via quenching of primary production and ii) positive feedback on anoxia via the promotion of DDA growth. The relative importance of either feedback mode depends on local conditions and is affected by niche segregation of N-loss and N_2-fixating microorganisms and nutrient availability (*e.g.*, phosphorous) in the euphotic zone. Our findings highlight that disentangling the coupling between N-loss processes and N_2-fixation is imperative to understanding the cascading effects of marine deoxygenation on biogeochemical cycling and potential feedback mechanisms on water column oxygenation.

5. Conclusions

By comparing biomarker information with redox proxies (redox sensitive trace metals and benthic foraminifer assemblages) in the presented EMS record, we show that a cascade of N-cycling shifts with various feedback modes on anoxia occurred during S1a, S1b and 'S2'. Lipid biomarkers show that Thaumarchaeota were predominantly present in S1a, potentially promoted by enhanced nutrient availability via increased river discharge. Anammox intensity increased during S1, likely in response to the progressive deoxygenation of the SIW. Associated loss of bioavailable N may have fueled the ensuing increase in diatom-diazotroph associations (DDAs). In turn, this may have promoted enhanced remineralization rates via an increased flux of OM to the sea-floor, providing a positive feedback on anoxia (as has been proposed to occur in S4, S5 and S74 sapropels). During S1b, however, while anammox biomarker concentrations are equal to S1a, no evidence for such feedback is observed. A return to more oligotrophic conditions likely resulted in a P-limitation for diazotrophs. Under such conditions, the occurrence of anammox bacteria may have induced a negative feedback on anoxia, by quenching primary production, and hence, limiting the OM flux to the seafloor.

From ~69 to 39 cal ka BP, the occurrence of ladderanes and hexose HGs suggests episodes of bioavailable N removal via anammox bacteria and N_2-fixation by Nostocales, respectively, corresponding to recorded intervals of enhanced river activation. The low Ba/Al ratio indicates limited organic C export, and consequently, no significant increase in primary production. Hence, the short-lasting humid events recorded during this interval may not have been sufficient to reach the tipping point for true sapropel formation. Yet, foraminifer assemblages and Mn/Al do suggest brief periods of anoxia during these intervals (maximum deoxygenation at ~53–52 ka BP, *i.e.* timing of 'S2'), with the redoxcline being located around the sediment–water interface. During these intervals, ladderanes co-occur with BHT-34*R*. Compound-specific $\delta^{13}C_{BHT\text{-}34R}$ values indicate an anammox source, potentially synthesized by

marine anammox bacteria living in the nitrite-ammonium transition zone of marine sediments. As such, the large niche-segregation with primary producers likely resulted in a decoupling between N-loss and N_2-fixation at this time. In addition, the oligotrophic conditions (with extreme P-depletion) are thought to have also limited the presence of DDAs, as no pentose HGs were detected. Our results show various modes of operation of the N-cycle during different states of deoxygenation. Nutrient-availability and microbial niche-segregation are thought to strongly impact feedbacks of the N-cycle, which therefore necessitates considerations when assessing biogeochemical responses to marine deoxygenation.

Declaration of Competing Interest

The authors declare that they have no known competing financial interests or personal relationships that could have appeared to influence the work reported in this paper.

Data availability

All data related to this article is available online via doi: https://dataportal.nioz.nl/doi/10.25850/nioz/7b.b.fd.

Acknowledgement

We kindly thank the captain and crew of the R/V Pelagia for facilitating the collection of all sampled material during expedition 64PE406. Jessica Riekenberg is greatly appreciated for her contribution to the Bligh and Dyer lipid extractions. We further thank Ronald van Bommel for his help in the isotope lab. We are also very grateful for the support of Denise Dorhout and Monique Verweij during UHPLC-MS measurements. This research was supported by the Soehngen Institute of Anaerobic Microbiology (SIAM) Gravitation Grant (024.002.002) and the NESCC Gravitation Grant (024.002.001), awarded to JSSD by the Dutch Ministry of Education, Culture and Science (OCW). This work also benefited from data produced by the SCANALOGUE-project (ALWOP. 2015.113) awarded to GJR by the Netherlands Organization for Scientific Research (NWO).

Appendix A. Supplementary material

The supplementary material includes two files. The first file (supplementary material 1) describes the core chronology (S1.1) and figures of $\delta^{18}O$ values of *G. ruber* (Fig. S1), lipid biomarker concentrations normalized against TOC (Fig. S2), mass chromatograms and MS^2 of ladderanes (S3), mass chromatograms of FAME standards (Fig. S4), relative abundances of benthic foraminifers (Fig. S5). The second file (supplementary material 2) provides six tables with the data presented in the manuscript, in which table 1 presents the bulk sedimentary carbon and nitrogen data, table 2 to 5 the lipid biomarker accumulation rates and table 6 the benthic foraminiferal data. Supplementary material to this article can be found online at https://doi.org/10.1016/j.gca.2023.06.018.

References

Abu-Zied, R.H., Rohling, E.J., Jorissen, F.J., Fontanier, C., Casford, J.S.L., Cooke, S., 2008. Benthic foraminiferal response to changes in bottom-water oxygenation and organic carbon flux in the eastern Mediterranean during LGM to Recent times. Mar. Micropaleontol. 67, 46–68.

Algeo, T.J., Liu, J., 2020. A re-assessment of elemental proxies for paleoredox analysis. Chem. Geol. 540.

Andersen, M.B., Matthews, A., Bar-Matthews, M., Vance, D., 2020. Rapid onset of ocean anoxia shown by high U and low Mo isotope compositions of sapropel S1. Geochem. Perspect. Lett. 15, 10.

Azrieli-Tal, I., Matthews, A., Bar-Matthews, M., Almogi-Labin, A., Vance, D., Archer, C., Teutsch, N., 2014. Evidence from molybdenum and iron isotopes and molybdenum-uranium covariation for sulphidic bottom waters during Eastern Mediterranean sapropel S1 formation. Earth Planet. Sci. Lett. 393, 231–242.

Bale, N.J., Hopmans, E.C., Zell, C., Sobrinho, R.L., Kim, J.H., Sinninghe Damsté, J.S., Villareal, T.A., Schouten, S., 2015. Long chain glycolipids with pentose head groups as biomarkers for marine endosymbiotic heterocyte cyanobacteria. Org. Geochem. 81, 1–7.

Bale, N.J., Ding, S., Hopmans, E.C., Arts, M.G.I., Villanueva, L., Boschman, C., Haas, A.F., Schouten, S., Sinninghe Damsté, 2021. Lipidomics of Environmental Microbial Communities. I: Visualization of Component Distributions Using Untargeted Analysis of High-Resolution Mass Spectrometry Data. Front. Microbiol. 12, 659302.

Bale, N.J., Hennekam, R., Hopmans, E.C., Dorhout, D., Reichart, G.J., van der Meer, M., Villareal, T.A., Sinninghe Damsté, J.S., Schouten, S., 2019. Biomarker evidence for nitrogen-fixing cyanobacterial blooms in a brackish surface layer in the Nile River plume during sapropel deposition. Geology 47, 1088–1092.

Bar-Matthews, M., Ayalon, A., 2007. Speleothems as palaeoclimate indicators, a case study from Soreq Cave located in the Eastern Mediterranean Region, Israel. In: Battarbee, R.W. (Ed.), Past Climate Variability Through Europe and Africa. Kluwer Academic Publishers, Dordrecht, pp. 363–391.

Bauersachs, T., Compaoré, J., Hopmans, E.C., Stal, L.J., Schouten, S., Sinninghe Damsté, J.S., 2009. Distribution of heterocyte glycolipids in cyanobacteria. Phytochemistry 70, 2034–2039.

Bianchi, M., Fosset, C., Conan, P., 1999. Nitrification rates in the NW Mediterranean Sea. Aquat. Microb. Ecol. 17, 267–278.

Blanchet, C.L., Osborne, A.H., Tjallingii, R., Ehrmann, W., Friedrich, T., Timmermann, A., Brückmann, W., Frank, M., 2021. Drivers of river reactivation in North Africa during the last glacial cycle. Nat. Geosci. 14, 97–103.

Bligh, E.G., Dyer, W.J., 1959. A rapid method of total lipid extraction and purification. Can. J. Biochem. Physiol. 37, 911–917.

Calvert, S.E., 1983. Geochemistry of Pleistocene sapropels and associated sediments from the eastern Mediterranean. Oceanol. Acta 6, 255–267.

Castañeda, I.S., Schefuß, E., Pätzold, J., Sinninghe Damsté, J.S., Weldeab, S., Schouten, S., 2010. Millennial-scale sea surface temperature changes in the eastern Mediterranean (Nile River Delta region) over the last 27,000 years. Paleoceanography 25, PA1208.

Chiu, C.F., Sweere, T.C., de Clarkson, M.O., Souza, G.F., Hennekam, R., Vance, D., 2022. Co-variation systematics of uranium and molybdenum isotopes reveal pathways for descent into euxinia in Mediterranean sapropels. Earth Planet. Sci. Lett. 585, 117527.

Clarkson, M.O., Hennekam, R., Sweere, T.C., Andersen, M.B., Reichart, G.J., Vance, D., 2021. Carbonate associated uranium isotopes as a novel local redox indicator in oxidatively disturbed reducing sediments. Geochim. Cosmochim. Acta 311, 12–28.

Cornuault, M., Vidal, L., Tachikawa, K., Licari, L., Rouaud, G., Sonzogni, C., Revel, M., 2016. Deep water circulation within the eastern Mediterranean Sea over the last 95 kyr: New insights from stable isotopes and benthic foraminiferal assemblages. Palaeogeogr. Palaeoclimatol. Palaeoecol. 459, 1–14.

De Corte, D., Yokokawa, T., Varela, M.M., Agogúe, H., Herndl, G.J., 2009. Spatial distribution of Bacteria and Archaea and amoA gene copy numbers throughout the water column of the Eastern Mediterranean Sea. ISME J. 3, 147–158.

De Lange, G.J., Thomson, J., Reitz, A., Slomp, C.P., Speranza Principato, M., Erba, E., Corselli, C., 2008. Synchronous basin-wide formation and redox-controlled preservation of a Mediterranean sapropel. Nat. Geosci. 1, 606–610.

Di Donato, V., Sgarrella, F., Sprovieri, R., Di Stefano, E., Martín-Fernández, J.A., Incarbona, A., 2022. High-frequency modification of the central Mediterranean seafloor environment over the last 74 ka. Palaeogeogr. Palaeoclimatol Palaeoecol. 593.

Ducassou, E., Mulder, T., Migeon, S., Gonthier, E., Murat, A., Revel, M., Capotondi, L., Bernasconi, S.M., Mascle, J., Zaragosi, S., 2008. Nile floods recorded in deep Mediterranean sediments. Quat. Res. 70, 382–391.

Ducassou, E., Migeon, S., Mulder, T., Murat, A., Capotondi, L., Bernasconi, S.M., Mascle, J., 2009. Evolution of the nile deep-sea turbidite system during the late quaternary: Influence of climate change on fan sedimentation. Sedimentology 56, 2061–2090.

Elling, F.J., Hemingway, J.D., Kharbush, J.J., Becker, K.W., Polik, C.A., Pearson, A., 2021. Linking diatom-diazotroph symbioses to nitrogen cycle perturbations and deep-water anoxia: Insights from Mediterranean sapropel events. Earth Planet. Sci. Lett. 571, 117110.

Filippidi, A., De Lange, G.J., 2019. Eastern Mediterranean deep water formation during sapropel S1: A reconstruction using geochemical records along a bathymetric transect in the Adriatic outflow region. Paleoceanogr. Paleoclimatology 34, 409–429.

Follett, C.L., Dutkiewicz, S., Karl, D.M., Inomura, K., Follows, M.J., 2018. Seasonal resource conditions favor a summertime increase in North Pacific diatom-diazotroph associations. ISME J. 12, 1543–1557.

Grant, K.M., Rohling, E.J., Bar-Matthews, M., Ayalon, A., Medina-Elizalde, M., Ramsey, C.B., Satow, C., Roberts, A.P., 2012. Rapid coupling between ice volume and polar temperature over the past 50,000 years. Nature 491, 744–747.

Grant, K.M., Grimm, R., Mikolajewicz, U., Marino, G., Ziegler, M., Rohling, E.J., 2016. The timing of Mediterranean sapropel deposition relative to insolation, sea-level and African monsoon changes. Quat. Sci. Rev. 140, 125–141.

Hamasaki, K., Shishikura, R., Suzuki, S., Shiozaki, T., Ogawa, H., Nakamura, T., Suwa, Y., 2018. Distribution and phylogeny of anaerobic ammonium-oxidizing (anammox) bacteria in the water column of the central Pacific Ocean. Deep. Res. Part II Top. Stud. Oceanogr. 156, 60–67.

Hamersley, M.R., Lavik, G., Woebken, D., Rattray, J.E., Lam, P., Hopmans, E.C., Sinninghe Damsté, J.S., Krüger, S., Graco, M., Gutiérrez, D., Kuypers, M.M.M., 2007. Anaerobic ammonium oxidation in the Peruvian oxygen minimum zone. Limnol. Oceanogr. 52, 923–933.

Handley, L., Talbot, H.M., Cooke, M.P., Anderson, K.E., Wagner, T., 2010. Bacteriohopanepolyols as tracers for continental and marine organic matter supply and phases of enhanced nitrogen cycling on the late Quaternary Congo deep sea fan. Org. Geochem. 41, 910–914.
Hemingway, J.D., Kusch, S., Shah, W., Polik, C.A., Elling, F.J., Pearson, A., 2018. A novel method to measure the 13C composition of intact bacteriohopanepolyols. Org. Geochem. 123, 144–147.
Hennekam, R., Jilbert, T., Schnetger, B., De Lange, G.J., 2014. Solar forcing of Nile discharge and sapropel S1 formation in the early to middle Holocene eastern Mediterranean. Paleoceanography 29, 343–356.
Hennekam, R., Donders, T.H., Zwiep, K., de Lange, G.J., 2015. Integral view of Holocene precipitation and vegetation changes in the Nile catchment area as inferred from its delta sediments. Quat. Sci. Rev. 130, 189–199.
Hennekam, R., van der Bolt, B., van Nes, E.H., de Lange, G.J., Scheffer, M., Reichart, G.J., 2020. Early-warning signals for marine anoxic events. Geophys. Res Lett 47 e2020GL089183.
Higgins, M.B., Robinson, R.S., Carter, S.J., Pearson, A., 2010. Evidence from chlorin nitrogen isotopes for alternating nutrient regimes in the Eastern Mediterranean Sea. Earth Planet. Sci. Lett. 290, 102–107.
Higgins, M.B., Wolfe-Simon, F., Robinson, R.S., Qin, Y., Saito, M.A., Pearson, A., 2011. Paleoenvironmental implications of taxonomic variation among δ15N values of chloropigments. Geochim. Cosmochim. Acta 75, 7351–7363.
Higgs, N.C., Thomson, J., Wilson, T.R.S., Croudace, I.W., 1994. Modification and complete removal of eastern Mediterranean sapropels by postdepositional oxidation. Geology 22, 423–426.
Hilgen, F.J., 1991. Astronomical calibration of Gauss to Matuyama sapropels in the Mediterranean and implication for the Geomagnetic Polarity Time Scale. Earth Planet. Sci. Lett. 104, 226–244.
Hopmans, E.C., Kienhuis, M.V.M., Rattray, J.E., Jaeschke, A., Schouten, S., Sinninghe Damsté, J.S., 2006. Improved analysis of ladderane lipids in biomass and sediments using high-performance liquid chromatography/atmospheric pressure chemical ionization tandem mass spectrometry. Rapid Commun. Mass Spectrom. 20, 2099–2103.
Hopmans, E.C., Smit, N.T., Schwartz-Narbonne, R., Sinninghe Damsté, J.S., Rush, D., 2021. Analysis of non-derivatized bacteriohopanepolyols using UHPLC-HRMS reveals great structural diversity in environmental lipid assemblages. Org. Geochem. 160.
Howell, M.W., Thunell, R.C., 1992. Organic carbon accumulation in Bannock Basin: evaluating the role of productivity in the formation of Eastern Mediterranean sapropels. Mar. Geol. 103, 461–471.
Ibello, V., Cantoni, C., Cozzi, S., Civitarese, G., 2010. First basin-wide experimental results on N2 fixation in the open. Geophys. Res. Lett. 37, L03608.
Jensen, M.M., Kuypers, M.M.M., Lavik, G., 2008. Rates and regulation of anaerobic ammonium oxidation and denitrification in the Black Sea. 53, 23–36.
Jorissen, F.J., 1999. In: Sen Gupta, B.K. (Ed.), Modern Foraminifera. Kluwer Academic Publisher, pp. 161–179.
Jorissen, F.J., Fontanier, C., Thomas, E., 2007. Paleoceanographical proxies based on deep-sea benthic foraminiferal assemblage characteristics. In: Hillaire-Marcel, C., de Vernal, A. (Eds.), Developments in Marine Geology. Elsevier, pp. 263–325.
Kalvelage, T., Jensen, M.M., Contreras, S., Revsbech, N.P., Lam, P., Günter, M., LaRoche, J., Lavik, G., Kuypers, M.M.M., 2011. Oxygen sensitivity of anammox and coupled N-cycle processes in oxygen minimum zones. PLoS One 6, e29299.
Kartal, B., Rattray, J., van Niftrik, L.A., van de Vossenberg, J., Schmid, M.C., Webb, R.I., Schouten, S., Fuerst, J.A., Sinninghe Damsté, J.S., Jetten, M.S.M., Strous, M., 2007. Candidatus "Anammoxoglobus propionicus" a new propionate oxidizing species of anaerobic ammonium oxidizing bacteria. Syst. Appl. Microbiol. 30, 39–49.
Kartal, B., De Almeida, N.M., Maalcke, W.J., Op den Camp, H.J.M., Jetten, M.S.M., Keltjens, J.T., 2013. How to make a living from anaerobic ammonium oxidation. FEMS Microbiol. Rev. 37, 428–461.
Kemp, A.E.S., Pearce, R.B., Koizumi, I., Pike, J., Rance, J.S., 1999. The role of mat-forming diatoms in the formation of Mediterranean sapropels. Nature 398, 57–61.
Kidd, R.B., Cita, M.B., Ryan, W.B.F., 1978. Stratigraphy of Eastern Mediterranean Sapropel Sequences Recovered during DSDP Leg 42A and Their Paleoenvironmental Significance. Initial Reports of the Deep Sea Drilling Project, 42 Pt. 1 U.S. Government Printing Office.
Kool, D.M., Talbot, H.M., Rush, D., Ettwig, K., Sinninghe Damsté, J.S., 2014. Rare bacteriohopanepolyols as markers for an autotrophic, intra-aerobic methanotroph. Geochim. Cosmochim. Acta 136, 114–125.
Krom, M.D., Emeis, K.C., Van Cappellen, P., 2010. Why is the Eastern Mediterranean phosphorus limited? Prog. Oceanogr. 85, 236–244.
Krom, M.D., Herut, B., Mantoura, R.F.C., 2004. Nutrient budget for the Eastern Mediterranean: Implications for phosphorus limitation. Limnol. Oceanogr. 49, 1582–1592.
Kuenen, J.G., Robertson, L.A., 1988. Ecology of nitrification and denitrification. In: Cole, J.A., Ferguson, S.J. (Eds.), The Nitrogen and Sulphur Cycles. Cambridge University Press, Cambridge, pp. 161–218.
Kuypers, M.M.M., Silekers, A.O., Lavik, G., Schmid, M., Jøorgensen, B.B., Kuenen, J.G., Sinninghe Damsté, J.S., Strous, M., Jetten, M.S.M., 2003. Anaerobic ammonium oxidation by anammox bacteria in the Black Sea. Nature 422, 608–611.
Kuypers, M.M.M., van Breugel, Y., Schouten, S., Erba, E., Sinninghe Damsté, J.S., 2004. N_2-fixing cyanobacteria supplied nutrient N for Cretaceous oceanic anoxic events. Geology 32, 853–856.
Kuypers, M.M.M., Lavik, G., Woebken, D., Schmid, M., Fuchs, B.M., Amann, R., Jørgensen, B.B., Jetten, M.S.M., 2005. Massive nitrogen loss from the Benguela upwelling system through anaerobic ammonium oxidation. Proc. Natl. Acad. Sci. U. S. A. 102, 6478–6483.
Lam, P., Jensen, M.M., Lavik, G., McGinnis, D.F., Müller, B., Schubert, C.J., Amann, R., Thamdrup, B., Kuypers, M.M.M., 2007. Linking crenarchaeal and bacterial nitrification to anammox in the Black Sea. Proc. Natl. Acad. Sci. U. S. A. 104, 7104–7109.
Langgut, D., Almogi-Labin, A., Bar-Matthews, M., Pickarski, N., Weinstein-Evron, M., 2018. Evidence for a humid interval at ~56–44 ka in the Levant and its potential link to modern humans dispersal out of Africa. J. Hum. Evol. 124, 75–90.
Laskar, J., Robutel, P., Joutel, F., Gastineau, M., Correia, A.C.M., Levrard, B., 2004. A long-term numerical solution for the insolation quantities of the Earth. Astron. Astrophys. 428, 261–285.
Lengger, S.K., Rush, D., Mayser, J.P., Blewett, J., Schwartz-Narbonne, R., Talbot, H.M., Middelburg, J.J., Jetten, M.S.M., Schouten, S., Sinninghe Damsté, J.S., Pancost, R.D., 2019. Dark carbon fixation in the Arabian Sea oxygen minimum zone contributes to sedimentary organic carbon (SOM). Global Biogeochem. Cycles 33, 1715–1732.
Mancini, A.M., Bocci, G., Morigi, C., Gennari, R., Lozar, F., Negri, A., 2023. Past analogues of deoxygenation events in the Mediterranean sea : a tool to constrain future impacts. Mar. Sci. Eng. 11, 562.
Mara, P., Mihalopoulos, N., Gogou, A., Daehnke, K., Schlarbaum, T., Emeis, K.C., Krom, M., 2009. Isotopic composition of nitrate in wet and dry atmospheric deposition on Crete in the eastern Mediterranean Sea GB4002. Global Biogeochem. Cycles 23, 1–11.
Matthews, A., Azrieli-Tal, I., Benkovitz, A., Bar-Matthews, M., Vance, D., Poulton, S.W., Teutsch, N., Almogi-Labin, A., Archer, C., 2017. Anoxic development of sapropel S1 in the Nile Fan inferred from redox sensitive proxies, Fe speciation, Fe and Mo isotopes. Chem. Geol. 475, 24–39.
Menzel, D., Hopmans, E.C., Schouten, S., Sinninghe Damsté, J.S., 2006. Membrane tetraether lipids of planktonic Crenarchaeota in Pliocene sapropels of the eastern Mediterranean Sea. Palaeogeogr. Palaeoclimatol. Palaeoecol. 239, 1–15.
Meyers, P.A., Negri, A., 2003. Introduction to "paleoclimatic and paleoceanographic records in Mediterranean sapropels and mesozoic black shales". Palaeogeogr. Palaeoclimatol. Palaeoecol. 190, 1–8.
Möbius, J., Lahajnar, N., Emeis, K.C., 2010. Diagenetic control of nitrogen isotope ratios in Holocene sapropels and recent sediments from the Eastern Mediterranean Sea. Biogeosciences 7, 3901–3914.
Muerdter, D.R., Kennett, J.P., Thunell, R.C., 1984. Late Quaternary sapropel sediments in the eastern Mediterranean Sea: Faunal variations and chronology. Quat. Res. 21, 385–403.
Pantoja, S., Repeta, D.J., Sachs, J.P., Sigman, D.M., 2002. Stable isotope constraints on the nitrogen cycle of the Mediterranean Sea water column. Deep. Res. Part I Oceanogr. Res. Pap. 49, 1609–1621.
Peiseler, B., Rohmer, M., 1992. Prokaryotic triterpenoids of the hopane series. Bacteriohopanetetrols of new side-chain configuration from Acetobacter species. J. Chem. Res. 298–299.
Pitcher, A., Villanueva, L., Hopmans, E.C., Schouten, S., Reichart, G.J., Sinninghe Damsté, J.S., 2011. Niche segregation of ammonia-oxidizing archaea and anammox bacteria in the Arabian Sea oxygen minimum zone. ISME J. 5, 1896–1904.
Polik, C.A., Elling, F.J., Pearson, A., 2018. Impacts of paleoecology on the TEX 86 sea surface temperature proxy in the pliocene-pleistocene Mediterranean Sea. Paleoceanogr. Paleoclimatol. 33, 1472–1489.
Powley, H.R., Krom, M.D., van Capellen, P., 2016. Circulation and oxygen cycling in the Mediterranean Sea: Sensitivity to future climate change. J. Geophys. Res. Ocean 121, 3010–3028.
Rattray, J.E., van de Vossenberg, J., Hopmans, E.C., Kartal, B., van Niftrik, L., Rijpstra, W.I.C., Strous, M., Jetten, M.S.M., Schouten, S., Sinninghe Damsté, J.S., 2008. Ladderane lipid distribution in four genera of anammox bacteria. Arch. Microbiol. 190, 51–66.
Ridame, C., Le Moal, M., Guieu, C., Ternon, E., Biegala, I.C., L'Huelguen, S., Pujo-Pay, M., 2011. Nutrient control of N2 fixation in the oligotrophic Mediterranean Sea and the impact of Saharan dust events. Biogeosciences 8, 2773–2783.
Rohling, E.J., Jorissen, F.J., de Stigter, H.C., 1997. 200 Year interruption of Holocene sapropel formation in the Adriatic Sea. J. Micropalaeontol. 16, 97–108.
Rohling, E.J., Marino, G., Grant, K.M., 2015. Mediterranean climate and oceanography, and the periodic development of anoxic events (sapropels). Earth-Sci. Rev. 143, 62–97.
Rosa-Putra, S., Nalin, R., Domenach, A.M., Rohmer, M., 2001. Novel hopanoids from Frankia spp. and related soil bacteria: Squalene cyclization and significance of geological biomarkers revisited. Eur. J. Biochem. 268, 4300–4306.
Rossignol-Strick, M., 1982. After the deluge: Mediterranean stagnation and sapropel formation. Nature 295, 105–109.
Rossignol-Strick, M., 1985. Mediterranean Quaternary sapropels, an immediate response of the African monsoon to variation of insolation. Palaeogeogr. Palaeoclimatol. Palaeoecol. 49, 237–263.
Rush, D., Jaeschke, A., Hopmans, E.C., Geenevasen, J.A.J., Schouten, S., Sinninghe Damsté, J.S., 2011. Short chain ladderanes: Oxic biodegradation products of anammox lipids. Geochim. Cosmochim. Acta 75, 1662–1671.
Rush, D., Hopmans, E.C., Wakeham, S.G., Schouten, S., Sinninghe Damsté, J.S., 2012. Occurrence and distribution of ladderane oxidation products in different oceanic regimes. Biogeosciences 9, 2407–2418.
Rush, D., Sinninghe Damsté, J.S., Poulton, S.W., Thamdrup, B., Garside, A.L., Acuña González, J., Schouten, S., Jetten, M.S.M., Talbot, H.M., 2014. Anaerobic ammonium-oxidising bacteria: A biological source of the bacteriohopanetetrol stereoisomer in marine sediments. Geochim. Cosmochim. Acta 140, 50–64.
Rush, D., Talbot, H.M., Van Der Meer, M.T.J., Hopmans, E.C., Douglas, B., Sinninghe Damsté, J.S., 2019. Biomarker evidence for the occurrence of anaerobic ammonium oxidation in the eastern Mediterranean Sea during Quaternary and Pliocene sapropel formation. Biogeosciences 16, 2467–2479.

Sachs, J.P., Repeta, D.J., 1999. Oligotrophy and nitrogen fixation during eastern Mediterranean sapropel events. Science 286, 2485–2488.
Sarmiento, J.L., Herbert, T., Toggweiler, J.R., 1988. Mediterranean nutrient balance and episodes of anoxia. Gobal Biogeochem. Cycles 2, 427–444.
Schouten, S., Strous, M., Kuypers, M.M.M., Rijpstra, W.I.C., Baas, M., Schubert, C.J., Jetten, M.S.M., Sinninghe Damsté, J.S., 2004. Stable carbon isotopic fractionations associated with inorganic carbon fixation by anaerobic ammonium-oxidizing bacteria. Appl. Environ. Microbiol. 70, 3785–3788.
Schouten, S., Villareal, T.A., Hopmans, E.C., Mets, A., Swanson, K.M., Sinninghe Damsté, J.S., 2013. Endosymbiotic heterocyte cyanobacteria synthesize different heterocyte glycolipids than free-living heterocyte cyanobacteria. Phytochemistry 85, 115–121.
Schwartz-Narbonne, R., Schaeffer, P., Hopmans, E.C., Schenesse, M., Charlton, E.A., Jones, D.M., Sinninghe Damsté, J.S., Farhan Ul Haque, M., Jetten, M.S.M., Lengger, S.K., Murrell, J.C., Normand, P., Nuijten, G.H.L., Talbot, H.M., Rush, D., 2020. A unique bacteriohopanetetrol stereoisomer of marine anammox. Org. Geochem. 143, 103994.
Sinninghe Damsté, J.S., Rijpstra, W.I.C., Reichart, G.J., 2002a. The influence of oxic degradation on the sedimentary biomarker record: II. Evidence from Arabian Sea sediments. Cosmochim. Acta 66, 2737–2754.
Sinninghe Damsté, J.S., Schouten, S., Hopmans, E.C., Van Duin, A.C.T., Geenevasen, J.A.J., 2002b. Crenarchaeol: The characteristic core glycerol dibiphytanyl glycerol tetraether membrane lipid of cosmopolitan pelagic crenarchaeota. J. Lipid Res. 43, 1641–1651.
Sinninghe Damsté, J.S., Strous, M., Rijpstra, W.I.C., Hopmans, E.C., Geenevasen, J.A.J., Van Duin, A.C.T., Van Niftrik, L.A., Jetten, M.S.M., 2002c. Linearly concatenated cyclobutane lipids form a dense bacterial membrane. Nature 419, 708–712.
Slomp, C.P., Thomson, J., De Lange, G.J., 2002. Enhanced regeneration of phosphorus during formation of the most recent eastern Mediterranean sapropel (S1). Geochim. Cosmochim. Acta 66, 1171–1184.
Strous, M., Van Gerven, E., Kuenen, J.G., Jetten, M., 1997. Effects of aerobic and microaerobic conditions on anaerobic ammonium- oxidizing (anammox) sludge. Appl. Environ. Microbiol. 63, 2446–2448.
Strous, M., Kuenen, J.G., Jetten, M.S.M., 1999. Key physiology of anaerobic ammonium oxidation. Appl. Environ. Microbiol. 65, 3248–3250.
Strous, M., Pelletier, E., Mangenot, S., Rattei, T., Lehner, A., Taylor, M.W., Horn, M., Daims, H., Bartol-Mavel, D., Wincker, P., Barbe, V., Fonknechten, N., Vallenet, D., Segurens, B., Schenowitz-Truong, C., Médigue, C., Collingro, A., Snel, B., Dutilh, B. E., Op Den Camp, H.J.M., Van Der Drift, C., Cirpus, I., Van De Pas-Schoonen, K.T., Harhangi, H.R., Van Niftrik, L., Schmid, M., Keltjens, J., Van De Vossenberg, J., Kartal, B., Meier, H., Frishman, D., Huynen, M.A., Mewes, H.W., Weissenbach, J., Jetten, M.S.M., Wagner, M., Le Paslier, D., 2006. Deciphering the evolution and metabolism of an anammox bacterium from a community genome. Nature 440, 790–794.
Sturt, H.F., Summons, R.E., Smith, K., Elvert, M., Hinrichs, K.U., 2004. Intact polar membrane lipids in prokaryotes and sediments deciphered by high-performance liquid chromatography/electrospray ionization multistage mass spectrometry - New biomarkers for biogeochemistry and microbial ecology. Rapid Commun. Mass Spectrom. 18, 617–628.
Talbot, H.M., Summons, R.E., Jahnke, L.L., Cockell, C.S., Rohmer, M., Farrimond, P., 2008. Cyanobacterial bacteriohopanepolyol signatures from cultures and natural environmental settings. Org. Geochem. 39, 232–263.
Thomson, J., Higgs, N.C., Wilson, T.R.S., Croudace, I.W., De Lange, G.J., Van Santvoort, P.J.M., 1995. Redistribution and geochemical behaviour of redox-sensitive elements around S1, the most recent eastern Mediterranean sapropel. Geochim. Cosmochim. Acta 59, 3487–3501.
Tribovillard, N., Algeo, T.J., Lyons, T., Riboulleau, A., 2006. Trace metals as paleoredox and paleoproductivity proxies: An update. Chem. Geol. 232, 12–32.
Van Cappellen, P., Powley, H.R., Emeis, K.C., Krom, M.D., 2014. A biogeochemical model for phosphorus and nitrogen cycling in the Eastern Mediterranean Sea: Part 1: Model development, initialization and sensitivity. J. Mar. Syst. 139, 460–471.
van de Graaf, A.A., de Bruijn, P., Robertson, L.A., Jetten, M.S.M., Kuenen, J.G., 1997. Metabolic pathway of anaerobic ammonium oxidation on the basis of ^{15}N studies in a fluidized bed reactor. 143, 2415–2421.
van de Vossenberg, J., Rattray, J.E., Geerts, W., Kartal, B., van Niftrik, L., van Donselaar, E.G., Sinninghe Damsté, J.S., Strous, M., Jetten, M.S.M., 2008. Enrichment and characterization of marine anammox bacteria associated with global nitrogen gas production. Environ. Microbiol. 10, 3120–3129.
van Kemenade, Z.R., Villanueva, L., Hopmans, E.C., Kraal, P., Witte, H.J., Sinninghe Damsté, J.S., Rush, D., 2022. Bacteriohopanetetrol-x: constraining its application as a lipid biomarker for marine anammox using the water column oxygen gradient of the Benguela upwelling system. Biogeosciences 19, 201–221.
van Santvoort, P.J.M., de Lange, G.J., Thomson, J., Cussen, H., Wilson, T.R.S., Krom, M. D., Ströhle, K., 1996. Active post-depositional oxidation of the most recent sapropel (S1. in sediments of the eastern Mediterranean Sea. Geochim. Cosmochim. Acta 60, 4007–4024.
van Santvoort, P.J.M., de Lange, G.J., Langereis, C.G., Dekkers, M.J., Paterne, M., 1997. Geochemical and paleomagnetic evidence for the occurrence of "missing" sapropels in eastern Mediterranean sediments. Paleoceanography 12, 773–786.
van Winden, J.F., Talbot, H.M., Kip, N., Reichart, G.J., Pol, A., McNamara, N.P., Jetten, M.S.M., Op den Camp, H.J.M., Sinninghe Damsté, J.S., 2012. Bacteriohopanepolyol signatures as markers for methanotrophic bacteria in peat moss. Geochim. Cosmochim. Acta 77, 52–61.
Vergnaud-Grazzini, C., Ryan, W.B.F., Cita, M.B., 1977. Stable isotopic fractionation, climate change and episodic stagnation in the Eastern Mediterranean during the late Quaternary. Mar. Micropaleontol. 2, 353–370.
Weldeab, S., Menke, V., Schmiedl, G., 2014. The pace of East African monsoon evolution during the Holocene. Geophys. Res. Lett. 41, 1724–1731.
Woebken, D., Fuchs, B.M., Kuypers, M.M.M., Amann, R., 2007. Potential interactions of particle-associated anammox bacteria with bacterial and archaeal partners in the Namibian upwelling system. Appl. Environ. Microbiol. 73, 4648–4657.
Woodward, J.C., Macklin, M.G., Krom, M.D., Williams, M.A.J., 2022. The Nile: evolution, quaternary river environments and material fluxes. In: Gupta, A. (Ed.), Large Rivers. John Wiley & Sons, Chichester, pp. 261–289.
Wörmer, L., Cirés, S., Velázquez, D., Quesada, A., Hinrichs, K.U., 2012. Cyanobacterial heterocyte glycolipids in cultures and environmental samples: Diversity and biomarker potential. Limnol. Oceanogr. 57, 1775–1788.
Wörmer, L., Lipp, J.S., Schröder, J.M., Hinrichs, K.U., 2013. Application of two new LC-ESI-MS methods for improved detection of intact polar lipids (IPLs) in environmental samples. Org. Geochem. 59, 10–21.
Yogev, T., Rahav, E., Bar-Zeev, E., Man-Aharonovich, D., Stambler, N., Kress, N., Béjà, O., Mulholland, M.R., Herut, B., Berman-Frank, I., 2011. Is dinitrogen fixation significant in the Levantine Basin, East Mediterranean Sea? Environ. Microbiol. 13, 854–871.
Zhao, R., Biddle, J.F., Jørgensen, S.L., 2022. Introducing Candidatus Bathyanammoxibiaceae, a family of bacteria with the anammox potential present in both marine and terrestrial environments. ISME Commun. 2.
Zirks, E., Krom, M.D., Zhu, D., Schmiedle, G., Goodman-Tchernov, B.N., 2019. Evidence for the Presence of Oxygen-Depleted Sapropel Intermediate Water across the Eastern Mediterranean during Sapropel S1. ACS Earth Sp. Chem. 3, 2287–2297.
Zirks, E., Krom, M., Schmiedl, G., Katz, T., Xiong, Y., Alcott, L.J., Poulton, S.W., Goodman-Tchernov, B.N., 2021. Redox evolution and the development of oxygen minimum zones in the Eastern Mediterranean Levantine basin during the early Holocene. Geochim Cosmochim Acta 297, 82–100.
Zwiep, K.L., Hennekam, R., Donders, T.H., van Helmond, N.A.G.M., de Lange, G.J., Sangiorgi, F., 2018. Marine productivity, water column processes and seafloor anoxia in relation to Nile discharge during sapropels S1 and S3. Quat. Sci. Rev. 200, 178–190.